united nations
educational, scientific
and cultural
organization

international atomic
energy agency

the
abdus salam
international centre for theoretical physics

SMR.1135 - 18

THIRD WORKSHOP ON
THIN FILMS PHYSICS AND TECHNOLOGY
(8 - 24 MARCH 1999)
including
TOPICAL CONFERENCE ON
MICROSTRUCTURE AND SURFACE MORPHOLOGY
EVOLUTION IN THIN FILMS
(24 - 26 MARCH 1999)

"Magnetometry of magnetic surfaces, interfaces and ultrathin films"

Giorgio ROSSI
University of Modena
Dipartimento di Fisica
Via Campi 213/a
I-41100 Modena
ITALY

LINEAR MAGNETIC DICHROISM IN DIRECTIONAL PHOTOEMISSION FROM CORE LEVELS AND VALENCE BANDS

Giorgio Rossi, [1,2] Fausto Sirotti, [1,2] and Giancarlo Panaccione [2]

[1]Laboratorium für Festkörperphysik, ETH-Zürich, CH-8093
[2]Laboratoire pour l'Utilisation du Rayonnement Electromagnetique, CNRS, CEA, MESR F-94305 Orsay

INTRODUCTION

The need for new surface specific probes of magnetism is very high. The ideal surface magnetic probe should be selectively sensitive to surface, subsurface and interface layers, atom-specific and site specific, i.e. sensitive to the local environment of the excited atom, an should provide an absolute measure of the magnetic moment associated to the selected atoms. The field of surface magnetism has been opened by the application of spin-polarimetry to photoelectrons and to the secondary electron yield.[1] The measure of spin polarization (SP) of secondaries is intrinsically surface sensitive due to the short escape depth for low energy photoelectrons in ferromagnets, and can be understood semi-quantitatively.[2] The magnetic resolution of SP is high and can be used for imaging surface magnetic domains[3] and for studying the dynamics of surface magnetism with time resolution in the picosecond range in laser experiments,[4] or in the nanosecond range in synchrotron radiation experiments.[5] SP of secondaries probes the average magnetization and cannot be made atom-specific without independent knowledge on the atomic structure.[6] Spin Polarized Low Energy Electron Diffraction is very surface sensitive,[7] but it is limited to ordered surfaces, and is not atom specific. The magneto-optic Kerr effect [8] is not surface sensitive and can be applied only to the study of ferromagnetic order in monolayers on non magnetic substrates.[9] The related X-ray techniques of circular magnetic dichroism and linear magnetic dichroism [10, 11] have the great advantage to be atom-specific [12] via the characteristic absorption thresholds, and allow for a quantitative derivation of orbital and spin moments via the application of sum rules on the X-ray absorption [13] and emission.[14] X-ray absorption is not surface sensitive: its application is limited to magnetic adlayers or multilayers. The basic spectroscopic tools of surface science, Auger electron spectroscopy and photoelectron spectroscopy of core levels and valence bands, have been implemented in the spin-resolved mode.[15, 16, 17] These are close to ideal tools for surface magnetism, but suffer for a great technical handicap: the low efficiency of spin-detection which is only some 10^{-3} and severely reduces the applications of these techniques. One reasonable approach to overcome these shortcomings is to develop highly efficient spin-detectors.[18, 19] An alternative is to exploit the properties of the dipole matrix elements for directional photoemission in order to probe magnetism via a dichroism approach.

The study of the Fano effect [20] implies the measure of the spin polarization of

Core Level Spectroscopies for Magnetic Phenomena: Theory and Experiment
Edited by Paul S. Bagus *et al.*, Plenum Press, New York, 1995

photoelectrons ejected from unpolarized atoms by circular polarized light. The same information can be obtained by performing a circular dichroism experiment on polarized atoms, with the great practical advantage of measuring an intensity difference, instead of a spin-polarization value.[21] The full angular distribution of photoelectrons ejected from polarized atoms contains all of the information sought in the photoemission experiment, without need of actually measuring the spin polarization of the photoelectrons. Cherepkov et Kuznetsov [22] suggested that the measure of differences of angular distributions, corresponding to polarization changes of the light, or of the initial atomic polarization, are a greatly simplified approach which allows to extract theoretical parameters from the photoemission experiments. Recently a discussion of the photoemission experiments in terms of fundamental spectra and their relationship with difference spectra, has been proposed by van der Laan and Thole.[23, 24] The specific interest in overcoming the need of spin-resolution in electron spectroscopy experiments on magnetic surfaces, and to avoid the use of circularly polarized soft X-rays, has led to the exploitation of the differences of angular distributions of photoelectrons in mirror experiments. Angle resolved experiments with linearly polarized light (as well as with unpolarized light) can be set up in a chiral geometry.[25] Mirror experiments can be obtained, for example, by reversing the initial state polarization of the atoms with an applied magnetic field. The differences in the angular distribution of photoelectrons between two mirror experiments are a special case of magnetic dichroism in photoemission.

PRINCIPLES

Embedding an atom in a magnetic field lowers its symmetry.

The magnetic field has axial symmetry. In an applied magnetic field the interaction between the field and the magnetic moment of the electrons in an atom splits the energy terms which correspond to the different possible values of the magnetic quantum number m. The atoms become polarized. In the limit of the anomalous Zeeman effect (the most general case for applied fields *weak* with respect to spin-orbit interaction of the electrons) the energy splitting of the lines is due to both S and L quantum numbers (LS coupling) i.e. by the total angular momentum quantum number J and are described by the effective gyromagnetic factors g_j : $\Delta E_{m,mj-1} = g_j \mu_B H_0$ where μ_B is the Bohr magneton and H_0 is the external field.[26] The light emission/absorption properties (i.e. the dipole transition selection rules $\Delta mj = 0, \pm 1$) for polarized atoms are anisotropic: in transversal observation (perpendicular to the direction of the applied magnetic field) three linear polarized lines are emitted (or absorbed) whilst in longitudinal observation (parallel to the field lines) two circular polarized lines are observed (absorbed) with opposite handedness ($\Delta mj = \pm 1$). This is shown in the textbook-like figures 1 and 2 for the D_2 transitions of Na atoms in a magnetic field: the magnetic sublevels of atoms embedded in external magnetic fields can be excited by absorption of circular polarized radiation of appropriate frequency in a longitudinal experiment (i.e. photon propagation direction parallel or antiparallel to the magnetization direction) and by linear polarized radiation in a transverse experiment, (i.e. photon propagation direction perpendicular to the magnetization axis).

The photoexcited atom of a ferromagnetic solid is polarized due to its embedment in the magnetic field of the neighboring atoms and in the crystal field. The photoemission final states are split by the exchange and coulomb interactions of the core hole with the exchange-split valence electrons, yielding a multiplet spectrum of magnetic sublevels. Average magnetic fields for bulk atoms are of the order of 10^3 Gauss. This implies a Zeeman splitting between adjacent mj sublevels of the order 10^{-4} eV. This value is small with respect to typical lifetime broadening of core levels and cannot be measured. The exchange interaction, on the other hand is typically four orders of magnitude larger. It induces different combinations of sublevels with respect to the Zeeman effect. LS coupling does not apply and spin-spin interaction dominates over spin-orbit. The inter-level energy splitting between these m sublevels of the order of 10^{-1} eV, which is clearly reflected in the photoemission lineshape.

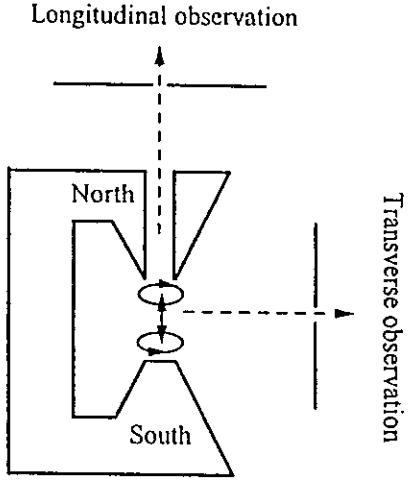

Fig.1: Transversal and longitudinal observation of emission lines from atoms in a magnetic field.

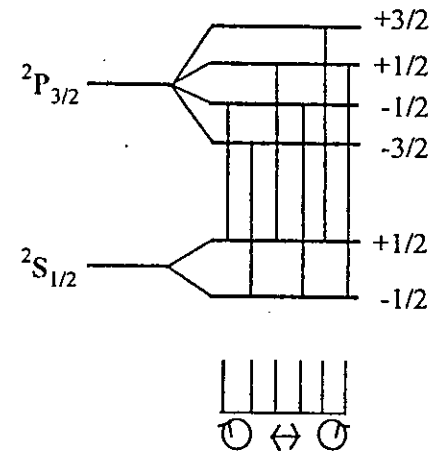

Fig.2: Anomalous Zeeman effect for alkali atoms. The D_2 spectrum is composed of six lines.

EXPERIMENTS

In figure 3 the 3p core level of Fe in *bcc*-Fe and in semiconducting β-$FeSi_2$ are compared. The silicide spectrum reflects the spin-orbit interaction in the open 3p core, with a splitting of $1.05 \pm .05 eV$ between a Fe $3p_{3/2}$ and Fe $3p_{1/2}$ peaks.[27] The spectrum of ferromagnetic *bcc*-Fe is much broader and asymmetric: it reflects the unresolved fine structure of magnetic and spin-orbit split sublevels. Spin-resolved experiments have shown that the fastest photoelectrons have minority spin character, whilst a peak of majority spin photoelectrons appears corresponding to the shoulder.[28]

In longitudinal photoemission experiments on ferromagnetic surfaces one aligns the propagation direction of circularly polarized radiation (q) with the macroscopic magnetization direction (M) of the sample surface.[29, 30, 31] The optical orientation of the photohole, due to the interaction of the photon spin with the hole orbit, is modulated by the electrostatic and exchange interactions with the spin-polarized valence band. By reversing the photon helicity the spectrum is dominated by the "other" set of interactions between the polarized hole (opposite spin) and the valence band. If this experiment is angle integrated then it is identical to exciting with a fixed helicity, and reversing the magnetization of the sample. In both cases the spectra corresponding to the interactions between hole and valence band have been separated as a function of core hole spin. This experiment is called Magnetic Circular Dichroism in photoemission, and yields information on the magnetization of the surface.[32, 24] In a transverse experiment one aligns the linearly polarized radiation (q) perpendicularly to the magnetization axis, so that also the linear polarization vector e is also perpendicular to M, therefore exciting all the magnetic sublevels. The spectral resolution of the magnetic sublevels in this case is limited by the magnitude of splitting, lifetime broadening and experimental energy resolution, obtaining the same magnetization averaged spectrum as the one of figure 3

for *bcc*-Fe. In fact these experiments are never exactly performed. This is due to the limited angular acceptance of the electron energy analyzer which operates a selection on the photoelectron emission directions (angle-resolved photoemission).[33] One therefore measures the angle distribution of the photoemission intensity, at the well defined angle set by the experimental geometry.

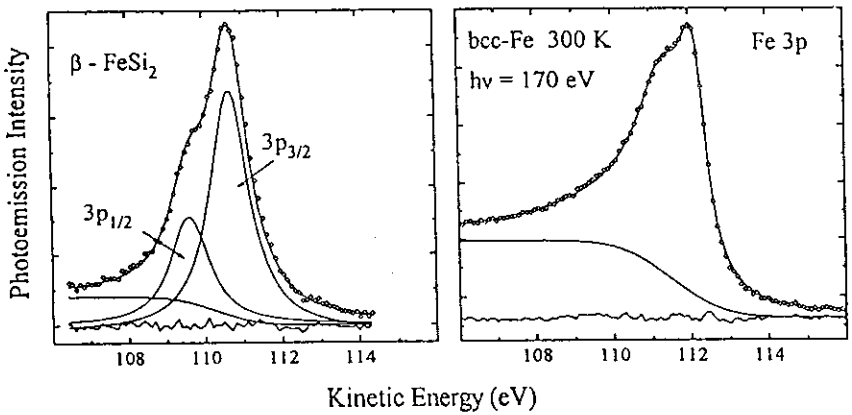

Fig.3: Photoelectron spectra of the Fe 3p core level in bcc-Fe (left) and in the semiconducting phase of iron-disilicide.(right) The semiconductor spectrum is easily decomposed in the two spin-orbit final states.

If the ferromagnetic sample is magnetized by an external field then its atoms have the axial symmetry of the field. The angular distribution of photoelectrons ejected from polarized atoms depends on three vectorial quantities, the direction of the photon beam q (or the direction of linear polarization e), the direction of photoelectron ejection k (or photoelectron momentum), and the direction of atomic polarization which, for a ferromagnetic surface, is given by the magnetization direction M. By choosing the photon direction as one axis of the laboratory frame, the angular distribution of the photoelectrons can be represented by a double expansion over spherical functions of two directions k and M.[34] In an angle resolved experiment the photoemission direction k is selected by the analyzer. The directional photoemission spectrum is different from the isotropic spectrum due to the interference between the dipole allowed final states which modify the directional photoemission intensity but not the angle integrated intensity due to complete averaging.[23, 35] The trick for doing a magnetization dependent experiment with angle-resolved photoemission (and without spin-resolution) is to fix the experimental geometry such to have a well defined chirality (i.e. to admit a distinct mirror experiment) and then to perform both the experiment and its mirror experiment obtained by reversing M, or by mirroring k. The difference of the two experiments is a difference between two angular distributions: it is a special photoemission magnetic dichroism called (Linear) Magnetic Dichroism in the Angular Distribution of photoelectrons [(L)MDAD].[36, 37, 38, 39, 40]

LMDAD experiments on Fe.

Let us consider a photoemission experiment in the geometry sketched in figure 4. It can be seen that two mirror experiments[25] are obtained depending on the magnetization direction oriented "above" the scattering plane (left handed triad, fig 4a) or "below" the scattering plane (right handed triad, fig 4b).

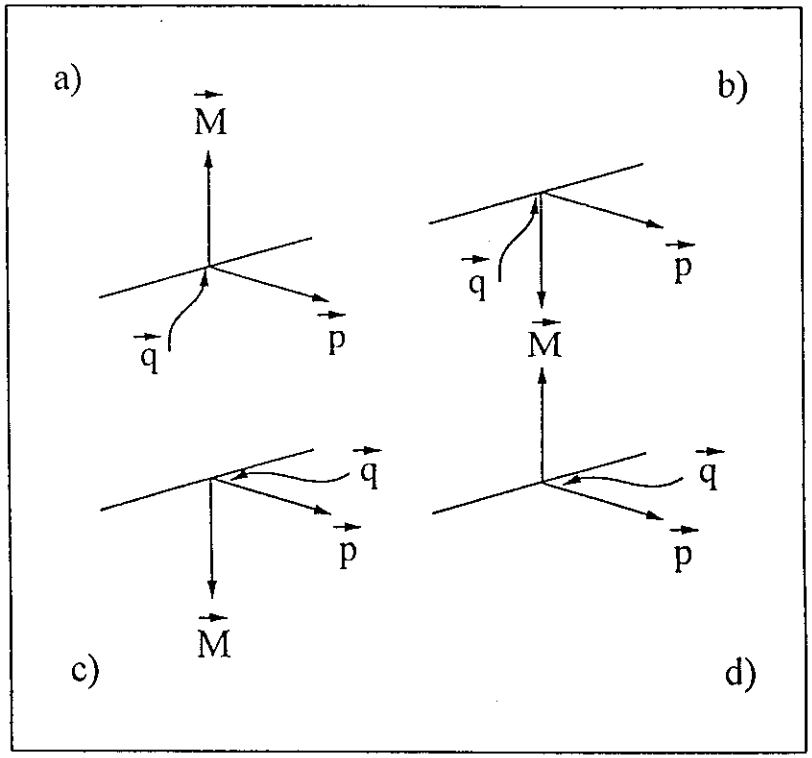

Fig.4: Geometry of the chiral experiment. Mirror experiments are obtained by reversal of M, (a,b) or by mirroring the photon beam direction.(a,d) Experiments (a,c) and (b,d) are identical.

The handedness of the experiment is reversed by reversing the surface magnetization on the sample (along the vertical axis). If the magnetization orientation is kept fixed mirror experiments can be obtained by impinging with the linear polarized photons from the "right" of the pM plane, instead than from the "left" (with the same incidence angle with respect to the photoelectron momentum, as seen in figure 4 a,b and b,c). More complex chiralities occur when more vector quantities enter in the experiment, like crystallographic symmetry directions that could be referred to the sample normal.[35, 41] The three vector chirality of the example is necessary and sufficient to do magnetic dichroism experiments with linear polarized light, and to show their equivalence to longitudinal experiments with circular polarized light.[34, 23] One should note that effects of chirality (even of hidden chiralities) are so large that all photoemission experiments are in fact chiral to some degree, unless the special case of co-linear vectors is approximated.[35] Figure 5 shows core level photoemission data on Fe obtained from experiments with linear polarized undulator radiation from the SuperAco SU7 monochromator in the geometry of figure 4. The magnetization could be imposed parallel or antiparallel to the y-axis direction by applying a current to the magnet coil. The photoelectrons were collected by a MAC-II Riber analyzer whose axis lies along the sample normal. The overall energy resolution was 350 meV for the valence band and 3p spectra and 500 meV for the 3s spectra.[38, 39]

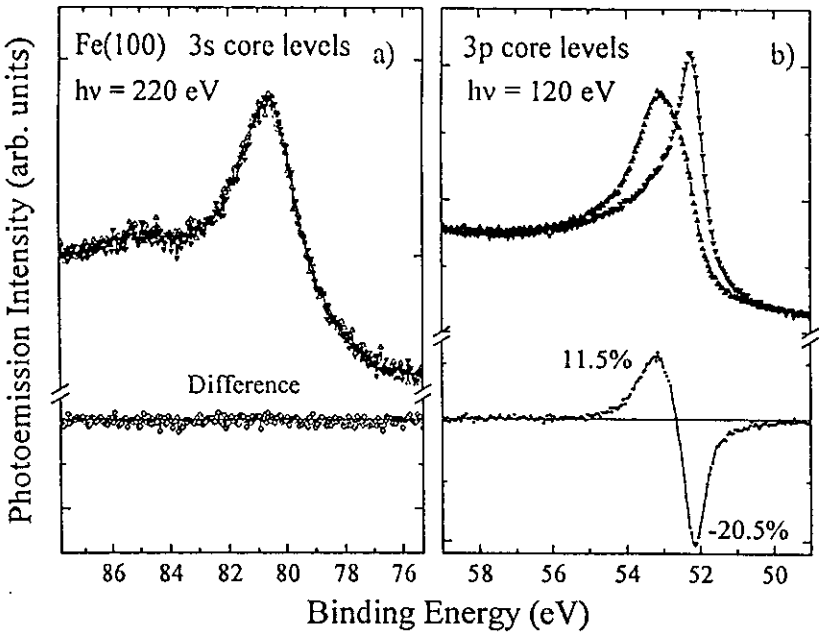

Fig.5: Fe 3s and Fe 3p core levels from Fe(100) as a function of magnetization reversal in a chiral experiment. The difference is zero for l=0 levels.

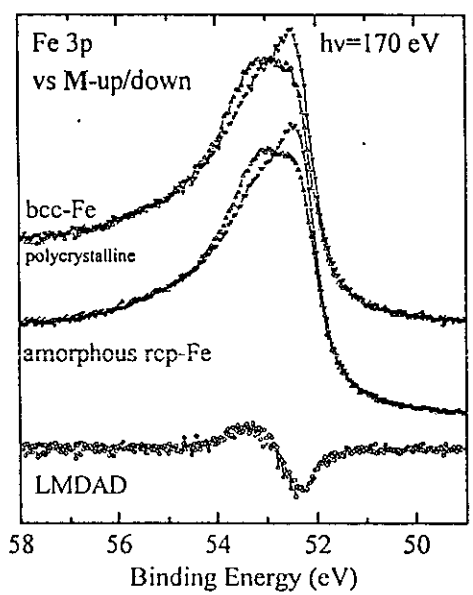

Fig.6: Fe 3p LMDAD measured in the same geometry from polycrystalline Fe and from amorphous rcp-Fe at 30 K.

-4-

Two spectra are shown as obtained for opposite directions of M and their difference. The left panel shows the 3s core level with its exchange split satellite at $-4.5eV$ [9] no difference is detected between the two magnetization directions. The right panel shows the 3p core levels, which display a large difference on the leading peak. The difference spectra are qualitatively identical for single crystal (100) surfaces of Fe, epitaxial *fcc*-Fe/Cu-Al(100), polycrystalline *bcc*-Fe, amorphous *rcp*-Fe and Fe in $Fe_4Ni_4B_2$. Some spectra are collected in figure 6. These data give directly two informations: a) Fe 3p core levels show magnetic dichroism upon magnetization reversal in chiral experiments. The effect is large giving a maximum asymmetry of 20% of the total intensity. The effect is connected with the axial symmetry of the magnetized sample, and is fully independent on the crystallographic environment or long range order. Finally the LMDAD signal is a difference signal of two Fe 3p photoemission spectra, i.e. it cost a factor of two more measurements than the standard core level photoemission with linearly polarized synchrotron radiation. This is the major advantage with respect to circular magnetic dichroism in photoemission, which requires circular polarized soft X-rays, usually less intense then the linearly polarized sources on synchrotron rings. The advantage over spin-detection is still larger since only photoemission intensity is measured.

b) $l = 0$ core levels, like Fe 3s, do not show LMDAD. This strongly indicates that the LMDAD is determined by the core hole, and not by the final photoelectron states.

LMDAD as a Kerr-like diagnostic tool

The first application of LMDAD is to probe the magnetic order at surfaces in a similar qualitative way as the magneto-optic Kerr effect probes the bulk magnetic order, but with the important advantage of chemical sensitivity. A clear example is given in figures 7 and 8. Fe 3p LMDAD gives a quick and direct evidence of the ferromagnetic order of the Fe(100) substrate surface, and of the ferromagnetic order and magnetization direction of the overlayers.

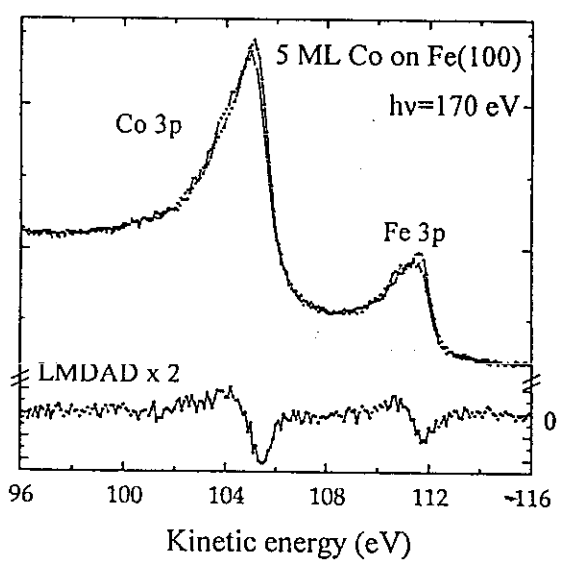

Fig.7: 3p core level spectra and LMDAD for epitaxial bcc-Co on Fe(100). The ferromagnetic coupling through the interface is seen by the same sign of LMDAD for the two elements.

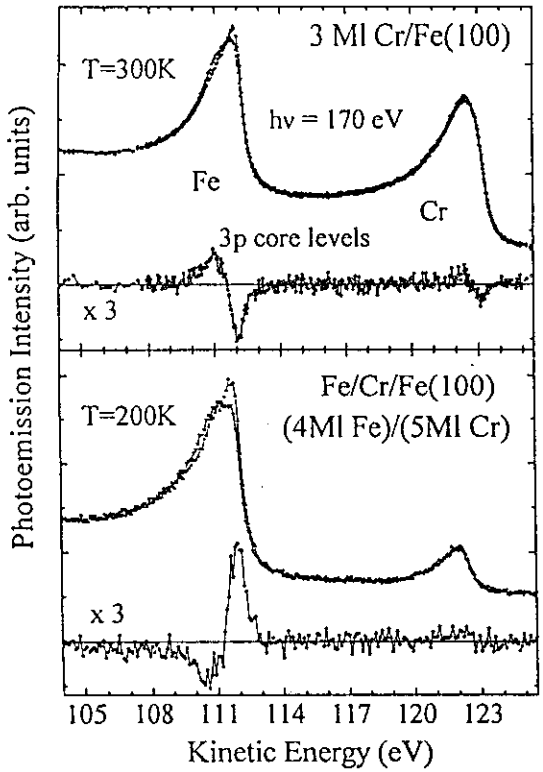

Fig.8: 3p spectra and LMDAD for epitaxial Cr/Fe(100) (top) and for a trilayer structure (bottom). The antiferromagnetic coupling of the Fe overlayer through the Cr spacer is seen by the reversal of the LMDAD asymmetry.

Figure 7 shows the LMDAD signal for 5 monolayers of *bcc*-Co epitaxially grown onto Fe(100) at 400K. Both Fe 3p and Co 3p show a similar dichroism indicating the ferromagnetic order of the bcc-Co overlayer and the ferromagnetic coupling across the interface. This information is obtained by only doubling the effort of measuring the core level lineshape, relative binding energy and relative intensity, as done in a standard XPS experiment. The LMDAD results for the growth of a Fe/Cr/Fe trilayer structure is shown in figure 8 : the top panel shows that the ferromagnetic order of the Fe(100) substrate is not disturbed by the epitaxial growth of 3 ML of Cr. The Cr 3p also shows LMDAD indicating ferromagnetic order in plane. Cr is known to grow along the [100] direction as a layered antiferromagnet,[43] the measured Cr 3p LMDAD is due to the uncompensated signal from the surface layer. The lower panel shows the completion of the trilayer structure by epitaxial overgrowth of Fe on a 5 ML thick Cr interlayer. The LMDAD signal shows that the top Fe film is antiferromagnetically coupled to the substrate iron across the 5 monolayers of chromium. The surface sensitivity of the photoemission was maximized by tuning the kinetic energy of the photoelectrons to the minimum of the escape depth. The same samples were studied in situ by $h\nu$-dependent SP measurements of the secondary yield. The SP averages over all the contribution to the yield, which include spin-polarized secondaries from the Fe overlayer, polarization-averaged emission from the Cr interlayers, spin filtering of the secondary

electrons traversing the Fe overlayer, spin-polarized secondaries from the Fe substrate attenuated through the Cr layers and filtered through the antiferromagnetically coupled Fe overlayer. This means that the SP results can be understood only by integrating independent knowledge on the structure of the trilayer, or with a model.[6]

The LMDAD of Fe 3p core levels is large enough to allow for magnetic hysteresis curves to be measured. This is expected to work on soft magnetic materials where the coercivity is of a few Gauss and the disturbance of the applied field to the photoelectron collection into the analyzer is small.

LMDAD of core levels as a surface magnetometer

The merit of core level LMDAD as a surface magnetometer can be addressed by the study of the temperature dependence of the Fe 3p LMDAD in an epitaxial ultrathin film. Four monolayers of *fcc*-Fe were epitaxially grown on *Cu-Al(100)*;[42] they could be remanently magnetized in plane. The LMDAD asymmetry as a function of sample temperature is shown in figure 9 where it is also compared with the mean field theory prediction for the behavior of ferromagnetism near the Curie temperature (T_c). By maximizing the linearity of $log[LMDAD]$ vs. $log[1 - T/Tc]$,[44] one finds a value of T_c = 288 K and a critical exponent $\beta = 0.212$ which are typical values for ultrathin Fe films.[45] The spread of the LMDAD points above T_c is due to the limited coherence of the ultrathin film, i.e. it represents the density of defects and domain boundaries in the film. LMDAD reflects therefore the average value of the magnetization $< M >$ and can be used to monitor surface magnetization likewise the SP of secondary electrons and the exchange asymmetry in SPLEED.[45]

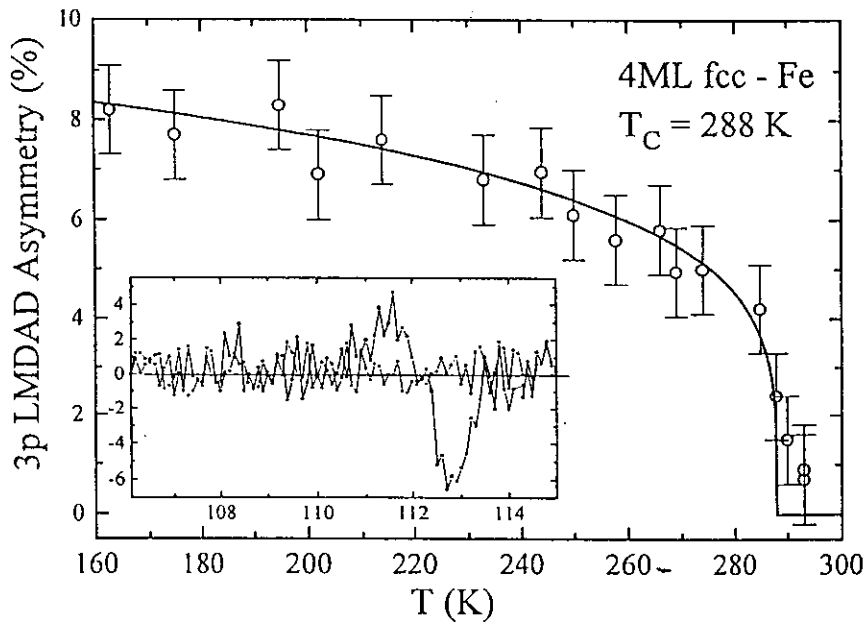

Fig.9: Temperature dependence of the Fe 3p LMDAD for an ultrathin epitaxial fcc-Fe layer grown on Cu-Al(100). The data are fitted by the mean field theory prediction. The LMDAD asymmetry at low and high temperatures are shown in the inset.

The obvious advantage of this probe over the other two since is the atom specificity and the chemical environment specificity via the core level chemical shifts. The surface sensitivity can be tuned by a proper choice of the photon energy. Also the presence of contaminants in the experiment can be easily monitored with photoemission and a reduction of LMDAD due to chemical reaction or contamination can be seen from a change of lineshape and presence of chemical shifts of the peak.

The absolute size of the LMDAD effect is on the other hand not well defined. It depends on the exact geometry of the experiment, the angular aperture of the electron spectrometer and on the photon energy employed and it can only be evaluated in the atomic model, disregarding all the solid state effects. This means that LMDAD cannot be an *absolute* surface magnetometer but its use is restricted to relative measurements of clean surfaces or adsorbates versus thickness, temperature, chemical reaction, etc. The LMDAD asymmetry in a given experiment can be calibrated against independent magnetic measurements, or against standard samples of known surface magnetic moments.

ATOMIC MODEL

Core level splitting

In ferromagnets the (3p,2p) core hole state of total angular momentum J is split by the exchange interaction with the (3d) valence electrons into sublevels with a given projection m_j on the magnetic quantization axis. We maintain this description of magnetic sublevels knowing that it is not an exact picture when considering the exchange interaction for which $J = L + S$ is not a good quantum number, i.e. the magnetic field cannot be treated as a perturbation of the spin-orbit splitting of the J levels, like in the anomalous Zeeman effect. So the m_j sublevels are the components of the splitting due to a *particular* magnetic field, the exchange field acting on spin only. The ordering of the m_j sublevels is different with respect to the Zeeman sublevel order, since exchange dominates over orbital interaction. By disregarding altogether the manybody processes involved in the photoemission from atoms and from solids, as well as the possible splitting of the high energy final states, one expects each m_j sublevel to contribute intensity with a characteristic angular distribution. In this case the core hole multiplet determines completely the intensity and the angular distribution of the photoemission spectrum. The advantage of this atomic model is that it places all of the emphasis on the matrix element for photoionization of a particular m_j core sublevel. This can be calculated within various possible schemes. Testing the atomic model of LMDAD[34] is rather straightforward since the relative variations of lineshape measured in the chiral photoemission experiment and in its mirror experiment, represent the relative variations of intensity from an effective grid of m_j sublevels. This can be compared with the relative magnitude of the calculated intensities for each m_j sublevel, for the specific chirality and photon energy.[39]

Since this model may appear too crude when we deal with photoemission from metals, a few comments are necessary. The photoexcitation of a core hole produces a multiplet of dipole allowed final states which reflect the configurations of the excited atom described by the interaction of the core holes with the conduction band holes. When localized open shells exist in the ground state of the atom, like the d-subshells in transition metals and the f-subshells in the rare earths and actinides, the interaction of the two open subshells can be so strong to spread the transition intensity over very broad multiplets with lots of structures. The intensity from a core level is therefore in general spread over several peaks and satellites. Experimentally one finds a variety of situations. Figure 10 shows extended spectra for Fe 3p and Ni 3p. The Ni 3p peak and satellites correspond to $3p^5d^{10}$, $3p^5d^9$ and $3p^5d^8$ final state configurations. The photoemission intensity of the satellites amounts to 20% of the total intensity. Since every configuration is different, it will display in principle a different magnetic dichroism.

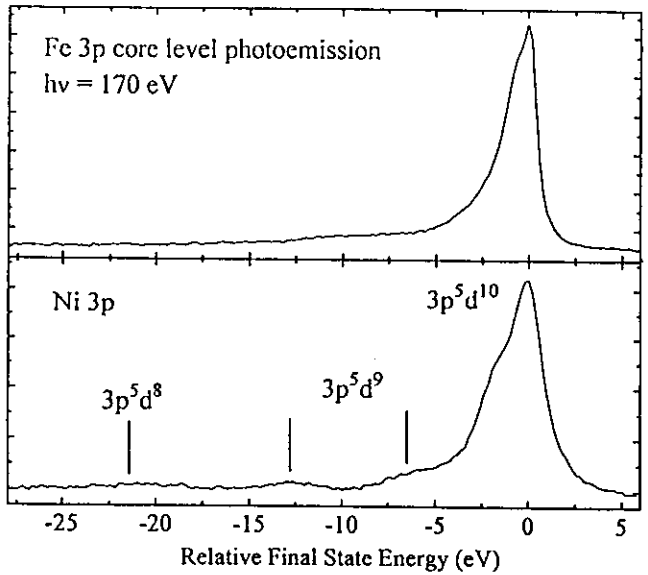

Fig.10: Wide range spectra of Fe 3p and Ni 3p core levels with evidence of satellites. Fe LMDAD (bottom).

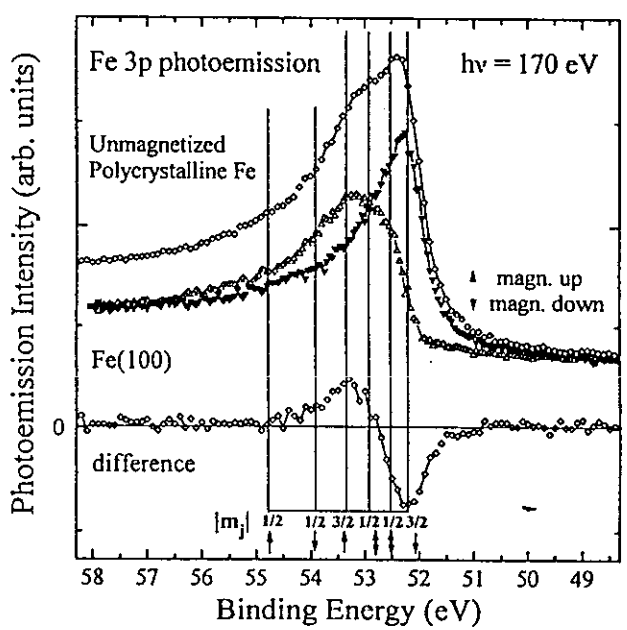

Fig.11: Fe 3p photoemission spectra after substraction of a common amount of unpolarized lineshape. The peaks and shoulders indicate a grid of magnetic sublevels.

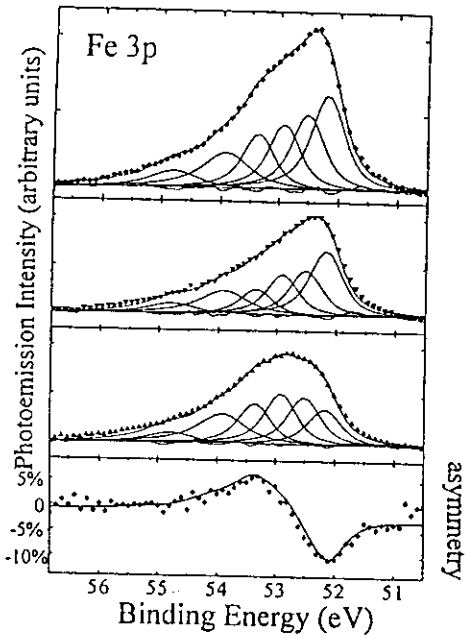

Fig.12: Analysis of the Fe 3p spectra with a sextuplet of Lorentian-Gaussian peaks with the parameters of table 1.

Such result has been suggested by a circular dichroism experiment on Ni.[46] In the case of Fe the measured photoemission intensity in the satellite region of the Fe 3p peak represents less then 10% of the total, and the maximum LMDAD asymmetry in the satellite region is less then 10^{-2}. This result for Fe 3p in *bcc*-Fe gives an empirical support to the discussion of the Fe 3p intensity as due to one dominant effective atomic configuration. Based on this facts one can attempt an analysis of the Fe 3p lineshape by adjusting a sextuplet of magnetic sublevels to the peaks and shoulders of the magnetization dependent spectra (figure 11). In the fitting procedure, whose results are shown in figure 12, the peak energies and amplitudes were constrained by the condition of simultaneously fitting the unmagnetized as well as the LMDAD spectra. The lineshapes and widths of each component of the sextuplet were kept fixed during the refinement procedure. The fitting parameters, and the results for the peak energies are collected in table 2. Systematically the deeper two states require a lorenzian broadening almost double with respect to the shallower four peaks.[39] One can notice that the spectral weight of the fitted sublevels deviates from a true atomic model. In fact the intensities of the $\pm m_j$ sublevels are not identical. The different intensity of the sublevels and their width (larger for the j=1/2 sublevels) are due to all the solid state effects which we have intentionally disregarded by adopting the atomic-like model. According to the atomic model the *sign and magnitude* of the variation of intensity of each peak as a function of the field reversal reflects the m_j character of each component.

The sublevels fitted to the unmagnetized spectrum are the atomic-like equivalent levels representing the 3p photoemission intensity in *bcc*-Fe. The goal of this analysis is to test the behavior of the sextet sublevels in the LMDAD experiment by comparing to the results of atomic calculations of the photoemission matrix elements. It is noteworthy

-7-

that a recent calculation of the density of states of 3p core levels in *bcc*-Fe gives a very similar sextuplet of sublevels to the one derived with our empirical procedure.[47]

State Multipoles

The angular distribution of photoelectrons can be represented by the density matrices [48] of both photon beam and initial atomic state.[34] A general expression for the angular distribution of photoelectrons ejected from polarized (i.e. axially symmetric) atoms was derived by [49, 22] introducing the atomic state multipoles. The state multipoles [34] describe the polarized core hole states, and also determine the angular distribution of the photoelectrons for a given polarization of the radiation. One consequence of this theory is that the sign and the magnitude of LMDAD for different magnetic sublevels is defined by the sign and the magnitude of the relevant state multipoles. By calculating the 3p state multipoles based on atomic wave functions and by comparing the results to the measured LMDAD asymmetry, a unique value of m_j can be attributed to each sublevel of the experimentally derived sextuplet. Therefore the LMDAD experiment identifies the components of the hole state with different projections m_j i.e. the fine structure of the 3p core holes in the presence of the exchange interaction. The state multipoles ρ^{n}_{N0} for each magnetic sublevel of p-states are given in Table 2.

For the geometry of the experiment shown in figure 4, the photoelectron current in a given direction, can be written using eq.(10) of ref.[22]:

$$I^{LMDAD}_{j} = I_j(\mathrm{M}) - I_j(-\mathrm{M}) = \frac{\sigma_{nlj}(\omega)}{2\pi} 3i\ \rho^{n}_{10}(2j+1)^{1/2}\ C^{j}_{221} \cdot \sin\vartheta\cos\vartheta$$

where M is the direction of the sample magnetization, $\sigma_{nlj}(\omega)$ is the photoionization cross section of the nlj subshell, ω is the photon energy, and ϑ is the angle of the grazing incidence of the light. The parameter C^{j}_{221} depends on the reduced dipole matrix elements for the transitions to the continuum states with $l-1$ and $l+1$ and on the corresponding phase shifts. In this approximation, neither the cross section σ_{nlj} nor the parameters C^{j}_{221} depend on m_j; therefore the sign and the relative magnitude of LMDAD for different magnetic sublevels is defined exclusively by the sign and the magnitude of the state multipoles ρ^{n}_{10}.

The comparison of theory and experiment is done in figures 13 and 14 for Fe 3p and Co 3p core levels in the pure metals.

Tab.1: Fitting parameters for the unmagnetized spectra of Fe 3p and Co 3p. The gaussian broadening was 350 meV and 500 meV for Fe and Co respectively.

	$Fe-3p$		$Co-3p$	
m_j	$B.E.(eV)$	$Lor.$	$B.E.(eV)$	$Lor.$
+3/2	52.2	0.42	59.6	0.7
+1/2	52.5	0.42	60.0	0.7
−1/2	52.9	0.42	60.5	0.7
−3/2	53.3	0.42	61.2	0.7
−1/2	53.9	0.85	61.8	1.0
+1/2	54.8	0.85	63.0	1.0

Tab .2: State multipoles ρ^{n}_{N0} for magnetic sublevels of $np_{1/2}$ and $np_{3/2}$ states.

	$j=1/2$		$j=3/2$			
m_j	+1/2	−1/2	+3/2	+1/2	−1/2	−3/2
ρ^{n}_{00}	$\frac{1}{\sqrt{2}}$	$\frac{1}{\sqrt{2}}$	$\frac{1}{2}$	$\frac{1}{2}$	$\frac{1}{2}$	$\frac{1}{2}$
ρ^{n}_{10}	$\frac{1}{\sqrt{2}}$	$-\frac{1}{\sqrt{2}}$	$\frac{3}{2\sqrt{5}}$	$\frac{1}{2\sqrt{5}}$	$-\frac{1}{2\sqrt{5}}$	$-\frac{3}{2\sqrt{5}}$
ρ^{n}_{20}	0	0	$\frac{1}{2}$	$-\frac{1}{2}$	$-\frac{1}{2}$	$\frac{1}{2}$
ρ^{n}_{30}	0	0	$\frac{1}{2\sqrt{5}}$	$-\frac{3}{2\sqrt{5}}$	$\frac{3}{2\sqrt{5}}$	$-\frac{1}{2\sqrt{5}}$

It allows to conclude that the magnetic sublevel level ordering is reversed with respect to the Zeeman splitting. This is understood as a consequence of the exchange coupling of the 3p core holes with the 3d band. [30, 29]

Fine Structure: Exchange and Spin-Orbit Parameters

From the fine structure of the 3p core levels one can evaluate the exchange splitting of the core hole. The width of the $J = 3/2$ multiplet is found here to be $1.11 \pm .05eV$ for Fe 3p, while the total width of the sextuplet is $2.6 \pm .1eV$. The spin orbit splitting of the 3p core holes in Fe and Co is known from silicide data [27] and is respectively $1.04 \pm .05eV$ and $1.43 \pm .05eV$ for Fe and Co. The splitting between adjacent m_j sublevels corresponds to a value of exchange field of 3.5 10^7 Gauss for the 3p core hole in *bcc*-Fe. It is noteworthy to stress here that chiral experiments including spin-polarization detection can be extended to nonmagnetic samples since the polarization of the initial state is replaced by the spin-polarization of the detected electrons. After the experiments of Schöhnense [50] on rare gases the technique has been applied to the valence band of Pt, measuring the spin-orbit interaction within the bands,[51] and on the 3p core level of fcc-Cu, which confirms exactly the atomic-like behavior.[52]

Spin-Selected Spectra:

With the knowledge of the fine structure of m_j levels projected along the magnetization direction M, one can reconstruct the energy distribution of the spin-selected Fe 3p spectra by making the proper linear combination of the individual m_j components of the sextuplet spectrum. The highest kinetic energy 3p sublevel has minority spin character, as it has been confirmed by spin-resolved photoemission experiments.[28, 16]

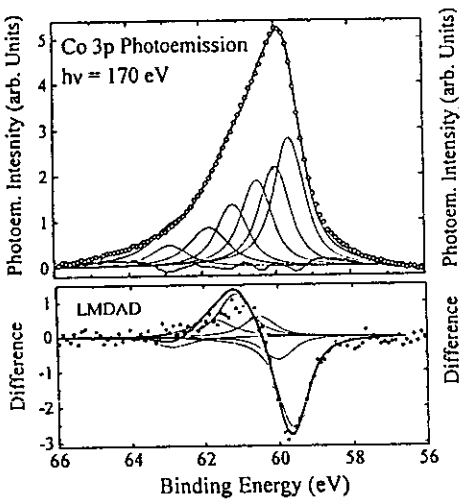

Fig.13: Upper panel: fitting of the Co 3p photoemission spectrum from unmagnetized Co (after integral background subtraction). In the bottom panel are shown the m_j components multiplied by the state multipoles of Table 2 along with the resulting convolution (continuous curve) and the experimental LMDAD spectrum (points).

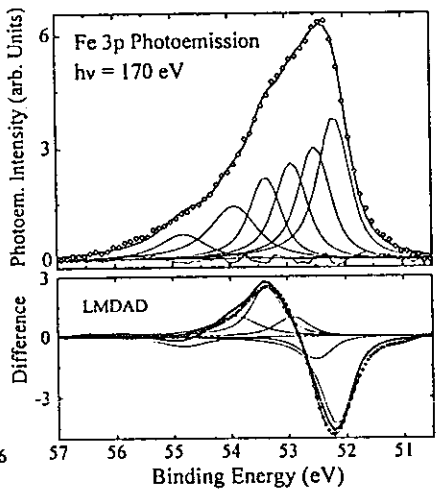

Fig.14:Upper panel: fitting of the Fe 3p photoemission spectrum from unmagnetized bcc Fe (after integral background subtraction). In the bottom panel are shown the m_j components multiplied by the state multipoles of Table 2 along with the resulting convolution (continuous curve) and the experimental LMDAD spectrum

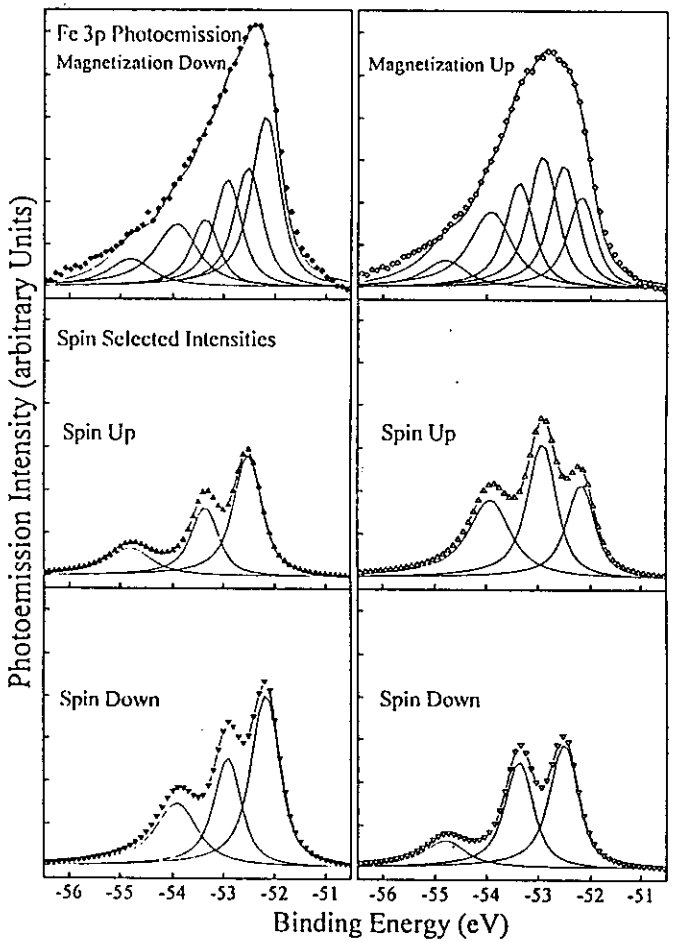

Fig.15:Experimental Fe 3p lineshapes obtained with down and up magnetization directions (full and open diamonds respectively) and the sextuplet fit with the parameters of Table 2. The lower panels show the spin selected lineshapes obtained using the m_j components of the sextuplets according to both spin projection and magnetization direction (full up triangles represent the majority spin spectrum excited with down magnetization, etc.). The curves can be directly compared to the spin-resolved experimental data of ref. 36

We approximate the $J = 3/2$, $m_j = \pm 3/2$ to pure spin states of minority (+) and majority (-) character. The intensity of the $J = 3/2$, $m_j = \pm 1/2$, and the $J = 1/2$, $m_j = \pm 1/2$ undefined spin states contains the linear combination of two spin states,[26] but for the geometry of this experiment only the components with projections of the angular momentum $m = \pm 1$ contribute.

With this procedure it becomes possible to reproduce spin-resolved angle integrated 3p spectra as well as spin-resolved LMDAD spectra based on the experimental intensities and widths of the sextuplet sublevels and on the calculated atomic LMDAD coefficients, as shown in figure 15. The lower panels show the LMDAD spin-selected intensities and

can be compared to the experimental results of Roth et al.[36] Apart a sign reversal, which is a mistake, the spectra are well reproduced and explained by our spin selected LMDAD lineshapes. By analyzing figures 15 one notices that a lack of symmetry is present in the spectra. Although the general spectral shape for opposite magnetization and opposite spin compare well, yet a complete symmetry, as expected for a dichroism experiment, is not observed. Figure 16 shows the total majority spin 3p intensity and minority spin 3p intensity for Fe: these spectra represent the spin selected photoelectron intensities as measured in a spin resolved photoemission experiment. The difference curve (I_{up} - I_{down}) and the spin-asymmetry ($I_{spin-up}$ - $I_{spin-down}$) / ($I_{spin-up}$ + $I_{spin-down}$) are also plotted. The results for Co are shown in figure 17. The area ratios for the (angle integrated) minority and majority spin 3p spectra are 1.33 for Fe and 1.18 for Co. This lack of symmetry is connected with the net spin polarization of Fe 3p core level photoemission spectra confirmed by several experiments.

These shortcomings are due to the restriction of the analysis only to the main photoemission peak. On the other hand the maximum dichroism measured in the satellite region is less then 10^{-2} i.e. it is very small, and does not allow to conclude about the presence of spin polarization well below the main 3p peak. The spin neutrality of core level photoemission experiments is still an open problem.

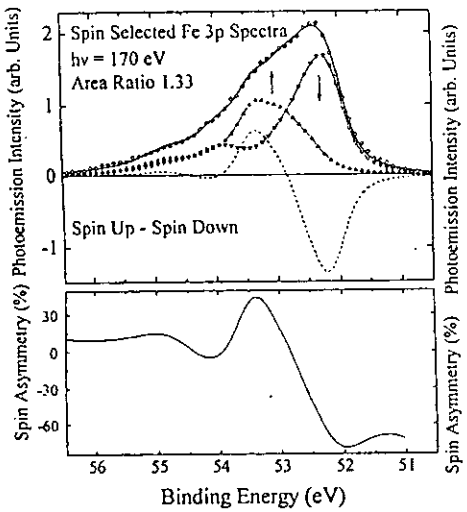

Fig.16: Spin-selected lineshapes obtained from the peaks of figure 15 by selecting all majority and minority spin intensities. Up (down) triangles indicate majority (minority) spins. The sum is compared to the unmagnetized spectrum (diamonds) The spin asymmetry is given at the bottom.

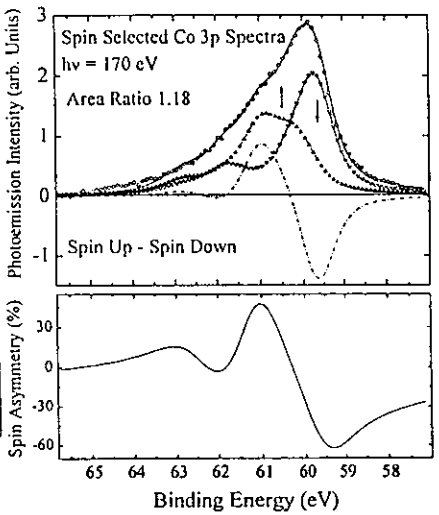

Figs.17: Spin-selected lineshapes of Co 3p core levels. Up (down) triangles indicate majority (minority) spins. The sum is compared to the unmagnetized spectrum (diamonds) The spin asymmetry is given at the bottom.

VALENCE BAND PHOTOEMISSION

LMDAD is also present in valence band photoemission experiments on Fe.[38] Figure 18 presents the 3d and valence band photoelectron energy distribution curves as obtained with excitation energy of $170eV$ and with the poor angle resolution of a cylindrical electron energy analyzer, i.e in a regime where the spectra represent the one hole density of states. The difference spectrum gives features across the whole d band. We therefore normalized the experimental intensity at $5eV$ binding energy, just below the bottom of the 3d band, in order to enhance the LMDAD signal from the background difference.

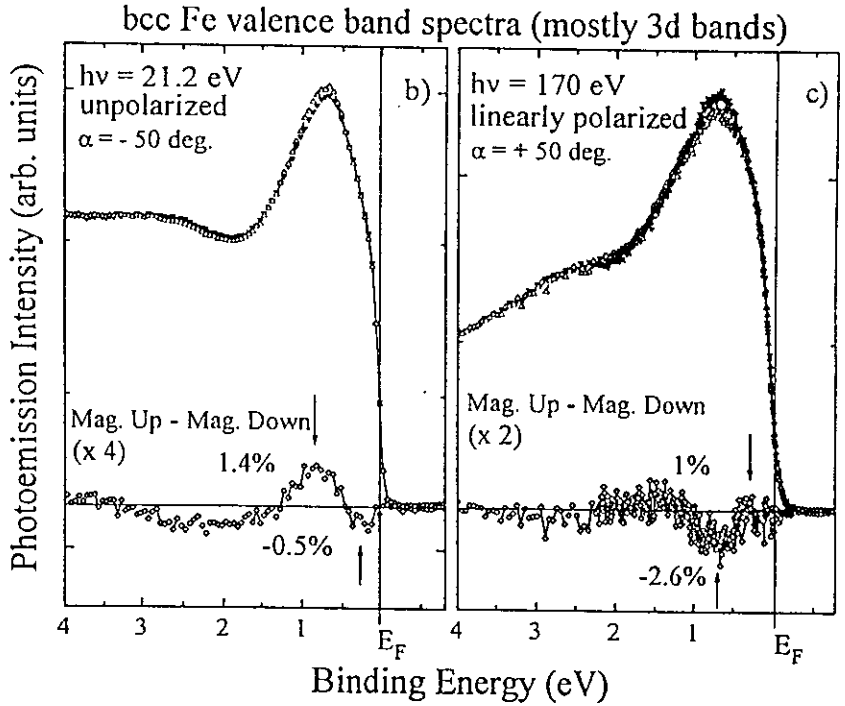

Fig.18: Valence band Fe 3d spectra and LMDAD as measured with linearly polarized synchrotron radiation,(a,b experiment following figure 4) and unpolarized He II radiation in a symmetric experiment.(d,c following figure 4)

The left panel of figure 18 shows a similar experiment performed with unpolarized Helium radiation at $21.2eV$ in the mirror geometry as the previous one, i.e. with the light beam impinging onto the sample from the opposite side of the pM plane.[53] The shape of the magnetization dependent spectra is different for $h\nu = 21.2eV$ and for $h\nu = 170eV$. This is due to the changes in the relative values of the photoionization cross sections for the 3d and the 4sp bands, and the different slope of the secondary electron distribution under the spectra. Nevertheless the shape of the difference spectra is very similar but inverted and roughly divided by two in the unpolarized ultraviolet spectrum. A narrow peak appears at $0.25eV$ below the Fermi level, and the main feature appears at about $0.75eV$. The asymmetry between 1.5 and $5eV$ is weak and it is sensitive to the exact alignment of the spectra, i.e .to the background intensity which is strong in the photoemission at the energy of He-I radiation ($h\nu = 21.2eV$). These results are consistent with the atomic theory for MDAD. In fact the sign reversal

of the MDAD asymmetry in the two experiments is due to the reversed chirality of the two experiments (the light sources impinge in the same plane but from opposite angles with respect to the photoelectron collection direction). Furthermore the factor of two reduction of the asymmetry in the IIe-I experiment reflects the use of unpolarized radiation, which can be viewed as the incoherent superposition of s and p linear polarized intensities. The $s-$polarized component is aligned with the magnetization and gives no MDAD effect,[36] and therefore only half of the unpolarized radiation contributes to the MDAD effect. One should remember, though, that the magnitude of the LMDAD effect also depends on photon energy, as measured and predicted in the soft X-rays range for the 3p subshell.[39] The reduction of LMDAD would be exactly a factor two if the same photon energy was used, and the effects of 100% $p-$polarized radiation vs. unpolarized radiation were compared. The same spectrum (at the same photon energy) can be obtained in the double-mirror experiment where M is inverted and q (e) is mirrored with respect to the pM plane. The experiments were repeated for polycrystalline *bcc*-Fe yielding the same results. This shows that the selection of special interband-transition and the electron state symmetry arguments put forwards to explain spin polarization in valence band photoemission from centrosymmetric surfaces are not necessary to explain LMDAD.[54] On the other hand the same experiment for amorphous *rcp*-Fe shows a qualitatively different LMDAD spectrum.[53] This means that the changes in the radial part of the 3d wavefunctions due to different hybridization do affect the LMDAD spectrum. The 3d peak position of *bcc*-Fe appears shifted by approximately $0.1eV$ when the magnetization is reversed. This shift is related to the spin-orbit interaction within the 3d band, which is the coupling mechanism for the spin and the photon field, i.e. the necessary interaction for the dichroism to occur.

The basic phenomenon is therefore the same as in core levels, and obeys to the same rules. The difference lies in the initial states which are represented by relativistic bands (in presence of exchange and spin-orbit interactions) instead of atomic-like levels. We note that similar results were obtained for Fe(100) and for fcc Co(001) by angular resolved photoemission with circular polarized synchrotron radiation at far-UV energies.[55, 56] The spectra showed Circular MDAD (CMDAD) asymmetries as a function of magnetization reversal, for a fixed light helicity, or as a function of helicity reversal for a fixed magnetization direction. The CMDAD spectra for Co(100) measured with $h\nu = 23eV$ [55] are very similar to our LMDAD results. The CMDAD results for Fe(100),[56] obtained with $h\nu = 31eV$ are also qualitatively the same. These facts are strong hints to the equivalence of LMDAD and CMDAD in valence band photoemission.[53] Experiments on Fe 3p core levels with circular and linear polarized light have been presented at this school by E. Kisker. Sum rules for photoemission with circularly polarized light from open shells have been derived, in analogy with the sum rules for X-ray absorption, but they are only valid for ideal angle integrated experiments.[57]

The valence bands chiral experiments show the generality of (L)MDAD in photoelectron spectroscopy which is not restricted to atomic-like core levels. This fact bears an analogy with the Cooper Minimum effect, which is an atomic property well described in photoionization from atoms, or from core-levels, but also measured in hybridized 4d and 5d valence bands of the transition metals, but with intensity changes in magnitude as a function of hybridization.[58]

Valence bands narrow at the surface in connection with the reduced neighbor coordinations of surface atoms. The d bands become therefore more localized and the orbits can partially relax, due to the reduced symmetry with respect to the bulk.The relaxation at the surface of the quenching of the orbital magnetic moment was predicted [59] and recently measured in the case of Ni.[46] The spin-orbit interaction of the 3d states at the surface should therefore in principle be different with respect to the bulk and enhance the LMDAD.

The (L)MDAD results on the valence bands of ferromagnets show that high resolution chiral photoemission experiments with unpolarized ultraviolet laboratory sources can be set up in such a geometry that a magnetic asymmetry can be detected. MDAD on 3p core levels with a laboratory X-ray source has also been demonstrated.[60]

CONCLUSIONS AND OUTLOOK

LMDAD is a large effect in chiral photoemission experiments on $l > 0$ initial states. The measure of LMDAD on core levels is a diagnostic of ferromagnetic order which cost only a double effort with respect to the standard photoemission lineshape inspection. This has, and will have a major impact on the spectroscopy of magnetic surfaces. The LMDAD asymmetry is directly proportional to $< M >$ and therefore it can be used to study the temperature dependence of ferromagnetic order at surfaces and the surface ferromagnetic hysteresis. The relation between the LMDAD asymmetry and the atomic magnetic moment is complex and, at present the only reliable quantities are the changes of the LMDAD asymmetry. The atomic calculations of LMDAD for the same subshell, say the 3p core level, of different atoms can be easily done and used to evaluate the relative results of LMDAD experiments, strictly done in the same geometry, on Fe, Co, Cr and the other transition metals. This should provide a guideline for the relative magnitudes of the magnetic moments if the solid state and manybody effects are not too different. The empirical transferability of the LMDAD asymmetry/magnetic moment ratio between Fe 3p and Co 3p appears to work, but preliminary results of Ni 3p are at odds, perhaps due to the larger satellite intensity of the Ni 3p spectrum.

Acknowledgements

This work was partially supported by the Swiss National Fund for Research, under program 24. We are in debt with N.A. Cherepkov and F. Combet Farnoux for their collaboration, and to H.C. Siegmann for stimulating comments and continuous support. One of us, G.P. acknowledges the EC for a grant under the Human Capital and Mobility Program.

References

[1] H.C. Siegmann; J. Phys.: Conden. Matter 4, 8395 (1992) and references quoted therein

[2] H.C. Siegmann, in this book

[3] R. Allenspach, J. Magn. Magn. Materials, 129, 160 (1994) and references therein

[4] A. Vaterlaus, T. Beutler, and F. Meier, Phys. Rev. Lett. 67, 3314 (1991)

[5] F. Sirotti, R. Bosshard, G. Panaccione, A. Jucha, and G. Rossi, to be published

[6] F. Sirotti, G. Panaccione, and G. Rossi, J. Physique, to be published

[7] J. Kirschner, in *Polarized Electrons in Surface Physics*, ed. by R. Feder, World Scientific, Singapore, 1985

[8] M.J. Freiser, IEEE Transactions on Magnetics, Mag-4, 152 (1968)

[9] T. Beier, H. Jahrreiss, D. Pescia, Th. Woike, and W. Gudat, Phys. Rev. Lett. 61, 1875 (1988)

[10] P. Carra and M. Altarelli, Phys. Rev. Lett. 64, 1286 (1990)

[11] M.Sacchi, F.Sirotti, G.Rossi, Solid State Commun. 81, 977 (1992); M. Sacchi, O. Sakho, F. Sirotti, and G. Rossi, Appl. Surf. Sci. 56-58, 1 (1992)

[12] C.T. Chen, Y.U. Idzerda, H.J. Lin, G. Meigs, A. Chaiken, G.A. Prinz, and G.H. Ho; Phys. Rev. **B48**, 642 (1993)

[13] B.T. Thole, P. Carra, F. Sette, and G. van der Laan; Phys. Rev. Lett. **68**, 1943 (1992)

[14] J. Stöhr and Y. Wu, in "New Directions in Research with Third Generation Soft X-Ray Synchrotron Radiation Sources" ed by. A.S. Schlachter and F. Wuillemier, 1994 Kluwer Academic Publisher p.221; F. Sette, ibid. p.251

[15] M. Landolt, in *Polarized Electrons in Surface Physics*, ed. by R. Feder, World Scientific, Singapore, 1985; R. Allenspach, D. Mauri, M. Taborelli, and M. Landolt, Phys. Rev. **B35**, 4801 (1987)

[16] C. Carbone, and E. Kisker; Solid State Commun. **65**, 1107 (1988)

[17] E. Kisker, in *Polarized Electrons in Surface Physics*, ed. by R. Feder, World Scientific, Singapore, 1985

[18] D. Tillmann, R. Thiel, E. Kisker, Z. Phys. B-Condensed Matter **77**, 1 (1989)

[19] G. Schönhense and H.C. Siegmann, Ann. Physik **2**, 465 (1993)

[20] U. Fano; Phys. Rev. **178**, 131 (1969)

[21] G. Baum, M.S. Lubell, and W. Raith, Phys. Rev. Lett. **25**, 267 (1970)

[22] N.A. Cherepkov and V.V. Kuznetsov J. Phys. B **22**, L405 (1989)

[23] G. van der Laan and B.T. Thole, Solid State Commun. **92**, 427 (1994

[24] B.T. Thole and G. van der Laan, Phys. Rev. Letters **67**, 3306 (1991); Phys. Rev. **B49**, 9613 (1994)

[25] G. Schönhense, Physica Scripta **T31**, 255 (1990)

[26] L.I. Schiff "Quantum Mechanics", McGraw-Hill New York (1955).

[27] F. Sirotti, M. De Santis, and G. Rossi, Phys. Rev. **B48**, 8299 (1993)

[28] B. Sinkovic, P.D. Johnson, N.B. Brookes, A. Clarke, and N.V. Smith, Phys. Rev. Lett. **65**, 1647 (1990)

[29] L. Baumgarten, C.M. Schneider, H. Petersen, F. Schafers, and J. Kirschner; Phys. Rev. Letters **65**, 492 (1990)

[30] H. Ebert, L. Baumgarten, C.M. Schneider, and J. Kirschner, Phys. Rev.B **44**, 4406 (1991)

[31] K. Starke, E. Navas, L. Baumgarten, and G. Kaindl, Phys. Rev. **B48**, 1329 (1993)

[32] G. van der Laan, Phys. Rev. Lett. **66**, 2527 (1991)

[33] N.V. Smith and P.K. Larsen; in *Photoemission and the Electron Properties of Surfaces* ed. by Feuerbacher, Fitton and Willis, John Wiley and Sons, New York, 1978.

[34] N.A. Cherepkov, Phys. Rev. B to be published; N.A. Cherepkov, V.V. Kuznetsov, and V.A. Verbitskii; J. Phys. B. to be published

[35] D. Venus; Phys. Rev. **B48**, 6144 (1993), ibid. **49**, 8821 (1994))

[36] Ch. Roth, F.U. Hillebrecht, H. Rose, and E. Kisker, Phys. Rev. Lett. **70**, 3479 (1993)

[37] Ch. Roth, H. Rose, F.U. Hillebrecht, and E. Kisker, Solid State Commun. **86**, 647 (1993)

[38] F. Sirotti and G. Rossi, Phys. Rev. **B49**, 15682 (1994)

[39] G. Rossi, F. Sirotti, N.A. Cherepkov, F. Combet Farnoux, and G. Panaccione, Solid State Commun. **90**, 557 (1994)

[40] E. Kisker, in this book

[41] C.M. Schneider, D. Venus, and J. Kirschner, Phys. Rev. **B45**, 5041 (1992)

[42] W. Macedo, A. Schatz, G. Panaccione, F. Sirotti, and G. Rossi, unpublished results

[43] J. Unguris, R.J. Celotta, and D. Pierce, Phys. Rev. Lett. **69**, 1125 (1992)

[44] D.L. Connelly, J.S. Loomis, and D.E. Mapother, Phys. Rev. **B3**, 924 (1971)

[45] W. Durr, M. Taborelli, O. Paul, R. Germar, W. Gudat, D. Pescia, and M. Landolt, Phys. Rev. Lett. **62**, 206 (1989)

[46] G. van der Laan, M.A. Hoyland, M. Surman, C.F. J. Flipse, and B.T. Thole, Phys. Rev. Lett **69**, 3827 (1993)

[47] E. Tamura, G.D. Waddill, J.G. Tobin, and P.A. Sterne, Phys. Rev. Lett. **73**, 1533 (1994)

[48] K. Blum, *Density Matrix Theory and Application* (Plenum, New York, 1981)

[49] H. Klar and H. Kleinpoppen, J. Phys. B **15**, 933 (1982)

[50] G. Schönhense, Phys. Rev. Lett. **44**, 640 (1980)

[51] N. Irmer, R. David, B. Schmeideskamp, and U. Heinzmann, Phys. Rev. **B45**, 3849 (1992)

[52] Ch. Roth, F.U. Hillebrecht, W.G. Park, H.B. Rose, and E. Kisker, Phys. Rev. Lett. **73**, 1963 (1994)

[53] G. Panaccione, F. Sirotti, and G. Rossi, to be published

[54] E. Tamura and R. Feder, Europhysics Lett. **16**, 695 (1991)

[55] C.M. Schneider, M.S. Hammond, P. Schuster, A. Cebollada, R. Miranda, and J. Kirschner, Phys. Rev. **B 44**, 12066 (1991)

[56] J. Bansmann, C. Westphal, M. Getzlaff, F. Fegel and G. Schonhense, J. Magn.Magn. Mater. **104-107**, 1691 (1992)

[57] B.T. Thole and G. van der Laan, Phys. Rev. Lett. **70**, 2499 (1993)

[58] G. Rossi, I. Lindau, L. Braicovich, and I. Abbati, Phys. Rev. **B 28**, 303 (1983)

[59] O. Eriksson, G.W. Fernando, R.C. Albers, and A.M. Boring, Solid. State Commun. **78**, 801 (1991)

[60] F.U. Hillebrecht, and W.D. Herberg, Z. Phys. **B93**, 299 (1994)

Time-resolved surface magnetometry in the nanosecond scale using synchrotron radiation

F. Sirotti,[a] R. Bosshard, P. Prieto,[b] and G. Panaccione[c]
Laboratoire pour l'Utilisation du Rayonnement Electromagnetique, CNRS-CEA-MESR, F-91405 Orsay, France

L. Floreano
INFM-TASC Laboratory, Area di Ricerca 99 Padriciano, I-34012 Trieste, Italy

A. Jucha and J. D. Bellier
Laboratoire pour l'Utilisation du Rayonnement Electromagnetique, CNRS-CEA-MESR, F-91405 Orsay, France

G. Rossi
Laboratorium für Festkörperphysik, ETH-Zürich, CH-8093, Switzerland;
INFM-Dipartimento di Fisica, Universitá di Modena, I-41100 Modena, Italy

(Received 15 July 1997; accepted for publication 25 October 1997)

The dynamics of magnetization reversal at surfaces and interfaces is studied by a specific photoelectric effect experiment with pulsed soft x rays. This novel time-resolved surface magnetometry is based on the measure of the spin polarization of the total photoejected electron yield by means of a Mott scattering experiment and on the acquisition synchronism with the multibunch structure of the positron storage ring SuperAco at Orsay (500 ps pulses at 120 ns intervals). We present results on the fast magnetization reversal of Fe ultrathin films deposited on amorphous low-coercivity ferromagnetic ribbons. © *1998 American Institute of Physics.* [S0021-8979(98)07303-4]

I. INTRODUCTION

Understanding the dynamics of magnetization at surfaces and interfaces is a prerequisite for a better description of fundamental and domain-mediated magnetic phenomena,[1–3] as well as for the tailoring of specific magnetic devices with the aim to increase the magnetic data exchange rate.

The effective coercivity of a ferromagnet depends upon the time scale of the process used to induce the magnetization reversal: by standard methods like vibrating -sample and 60 Hz magnetometers the time scale of 1 s and $10^{-5}-10^{-6}$ s respectively are accessible.[1,4] Experiments with 10^{-6} s resolution have been done on thin magnetic films by magnetooptical measures.[3,5] The technologically relevant time scale of 10^{-8} s has been reached by electrical measurements.[6,7] All of these techniques are sensitive to bulk magnetic properties and cannot be applied to surfaces, interfaces and atomically thin films (ATF). Actually the current trends in magnetism imply the study and the exploitation of mesoscopic particle size and atomically thin films in artificial structures in order to improve the recording resolution, the signal to noise ratio and the magnetic stability as well as the practical use of the specific magnetic properties of low-dimensional systems and of the stacking of atomically thin layers. A surface science approach to magnetometry is therefore quite appropriate, particularly if the surface sensitivity, and the sensitivity to small amounts of ferromagnetic matter can be coupled with time resolution on the relevant time scale.

We present in this article the principles and the demonstration of a novel approach to time resolved surface magnetometry based on spin polarization (SP) measurements of the time-resolved photoemission with two time scales accessible as a consequence of the photoexcitation source properties: single pulse resolution of 500 ps and real time measurements at 120 ns time intervals.

The photoexcitation process occurs on the 10^{-18} s time scale and the ejection of the so-called secondary electrons (i.e., Auger and scattered electrons) occurs within 10^{-15} s from the primary photoexcitation process so that the actual time resolution of a method based on the photoelectric effect is entirely set by the time duration of the excitation light pulse. The shortest available light pulses are from laser sources, routinely operated at ps or even sub-ps times. Pioneering experiments based on SP measurements with ps time resolution from a dye laser investigated the spin-lattice relaxation in Gd and Fe films.[8,9] The main limit to the application of the laser pulses comes from the photon energy, which is usually too low to photoexcite above the vacuum level of the material thus requiring special techniques for reducing the sample work function. Moreover, the maximum repetition rate is also limited. Synchrotron radiation (SR) from storage rings provides pulses of some tens of ps duration (30–50 ps from third generation sources, 200–500 ps from second generation sources like the one used in the present experiments) with an energy spectrum extending to x-ray energies and with repetition rates set by the operation

[a]Electronic mail: sirotti@LURE.U-PSUD.FR
[b]Present address: Dept. Fisica Aplicada, C-XII, Fac. De Ciencias, Univ. Autonoma de Madrid, 28049 Cantoblanco, Spain.
[c]Present address: Institut de Physique, Univ. Neuchâtel, CH-2001 Neuchâtel Switzerland.

 0021-8979/98/83(3)/1563/6/$15.00

mode of the storage ring, i.e., from a few ns up to several hundreds of ns. The surface sensitivity of this photoemission probe is achieved by the adequate energy selection of the electrons to be detected. The sensitivity to magnetism is then reached by a Mott scattering experiment which measures the SP of the ejected electron signal, without affecting the time scale of the experiment.[10] The magnetometry based on the SP measurement of secondary electrons photoexcited by SR[11] can fit the time domain relevant for many collective surface magnetic phenomena like reversal and reorientation processes, structural phase transitions, interdiffusion processes, growth processes, surface melting, etc. We report on the results obtained on the fast magnetization reversal of atomically thin Fe layers deposited in ultrahigh vacuum onto low-coercivity ferromagnetic ribbons.

II. EXPERIMENT

The time basis of the measurements was provided by the two-bunch operation of the SuperAco positron storage ring at Orsay providing pulses of 500 ps full width, at 120 ns intervals. The radiation source was the DOMINO undulator operated in wiggler mode illuminating the SU 7 beam line equipped with a TGM monochromator that was operated in total reflection mode therefore yielding polychromatic pulses of soft x rays. The photoelectrons ejected from the surface of the ferromagnetic sample after each SR pulse were accelerated to 100 kV kinetic energy and subsequently spin analyzed, along the direction specified by the magnetizing field, by means of a Mott scattering experiment[12] performed with a 100 kV Mott detector of the ETH-Zürich type.[13] Details of a Mott scattering setup can be found elsewhere.[14] The basic features of SP magnetometry with a Mott detector imply: (a) the collection of the total yield of the ejected electrons from a metal surface as a consequence of the photohole decay, (b) the formation of an electron beam and its acceleration up to 100 kV by means of a focusing electrostatic lens accelerator, (c) the scattering of the electron beam onto a thin gold target. Spin orbit scattering in the core electron field of the target determines a right-left asymmetry with respect to the quantization axis in space defined by the scattering plane of the Mott detector (which for our experiment coincides with the sample magnetization axis). The right-left asymmetry is defined as $A_{\text{Spin}}=(I_{\text{left}}-I_{\text{right}})/(I_{\text{left}}+I_{\text{right}})$ where $I_{\text{left (right)}}$ are the intensities measured by detectors positioned at 120° in the plane perpendicular to the quantization axis. The measured asymmetry, after correction by the Sherman function describing the scattering process and by the instrumental asymmetry, is proportional to the SP of the electrons emitted from the sample, i.e., to its average magnetization.[10] The surface sensitivity comes from the kinetic energy of the ejected electrons from the sample, which is of a few electron volts, as defined by the transmission function of the electrostatic lens accelerator.

The experiment is performed in ultrahigh vacuum (base pressure 4×10^{-10} mbar) on samples grown *in situ*, at temperatures in the range $T=150-300$ K. A typical hysteresis loop obtained from SP measurements in the usual operating mode, shows a remanent SP of ~15–25% (depending on Fe film thickness) and a coercive field of about 0.1 Oe, for Fe films of 1–5 nm thickness deposited on atomically clean (ion sputtered) surfaces of amorphous low-coercivity ferromagnetic Si-based alloys (commercial name: Vitrovac). A beam stopper, synchronized with the SP acquisition apparatus, let the surface to be exposed to the photon beam for less than one second during which time the acquisition is performed. This prevents a quick deterioration of the sample surface exposed to the high radiation power of the polychromatic SR beam. Details of the geometry and sample mounting can be found elsewhere.[15]

A schematic diagram of the experimental setup is shown in Fig. 1. SR impinges onto the sample at 45° with respect to the surface normal. The ejected yield within an emission cone of 10° around the sample normal is collected and accelerated towards the Au foil of the Mott scatterer. The clock of the experiment is referenced to the storage ring pulse structure by measuring with a pick-up induction device the passage of the particle bunches in the SuperAco storage ring: this pick-up signal is electronically shaped and transferred to the data acquisition system via an optical link. The whole measurement and data storage system is directly connected to the solid state detectors of the Mott scatterer at 100 kV with respect to ground. The silicon surface barrier detectors (PIPS-Canberra) output a pulse amplitude proportional to the number of detected electrons. The signal is preamplified with a total pulse width of about 60 ns and analog to digital converted by an 8 bits flash ADC, the resulting information is written automatically at the SuperAco frequency in a First In First Out (FIFO) 8192 bytes memory. A delay stage is introduced before the optical link of the clock (pick-up) signal in order to set the correct phase relationship between the electron pulses and the trigger signal.

The setup to reverse the magnetic field at high rate is schematically represented on the left of Fig. 1. The trigger to the magnetization reversal pulse is given synchronously with the SuperAco clock signal. At the beginning of a time-resolved measurement the sample is kept in one magnetization state by flowing a steady current (I_-) through the windings. Short magnetic field pulses are obtained by closing a fast high voltage transistor switch (Belcke type). When the switch is closed an extra current, delivered by the high voltage supply HV, is flowing through the windings. The magnetization reversal is obtained by selecting the amplitude of these two opposite currents. The rising time of such kind of pulses is of the order of a few ns for a pure resistor charge. The inductance L, introduced by the magnetic circuit which actually creates the magnetizing field applied to the sample, increases the pulse rising time. The time evolution of the applied magnetic field is shown in Fig. 2 for few values of the pulse current. The applied magnetic field reaches a stationary condition after 70 ns. This fact selects two classes of experiments: those in which one observes the magnetization reversal in constant applied field conditions (i.e., those for which the 100 ns raise time of H is a short time with respect to the dynamical response) and those experiments which measure the response of the surface magnetization to the time-varying magnetizing field, e.g., when the reversal occurs in a few tens of ns. This last class of experiment is in fact sensitive to the time derivative of the applied field

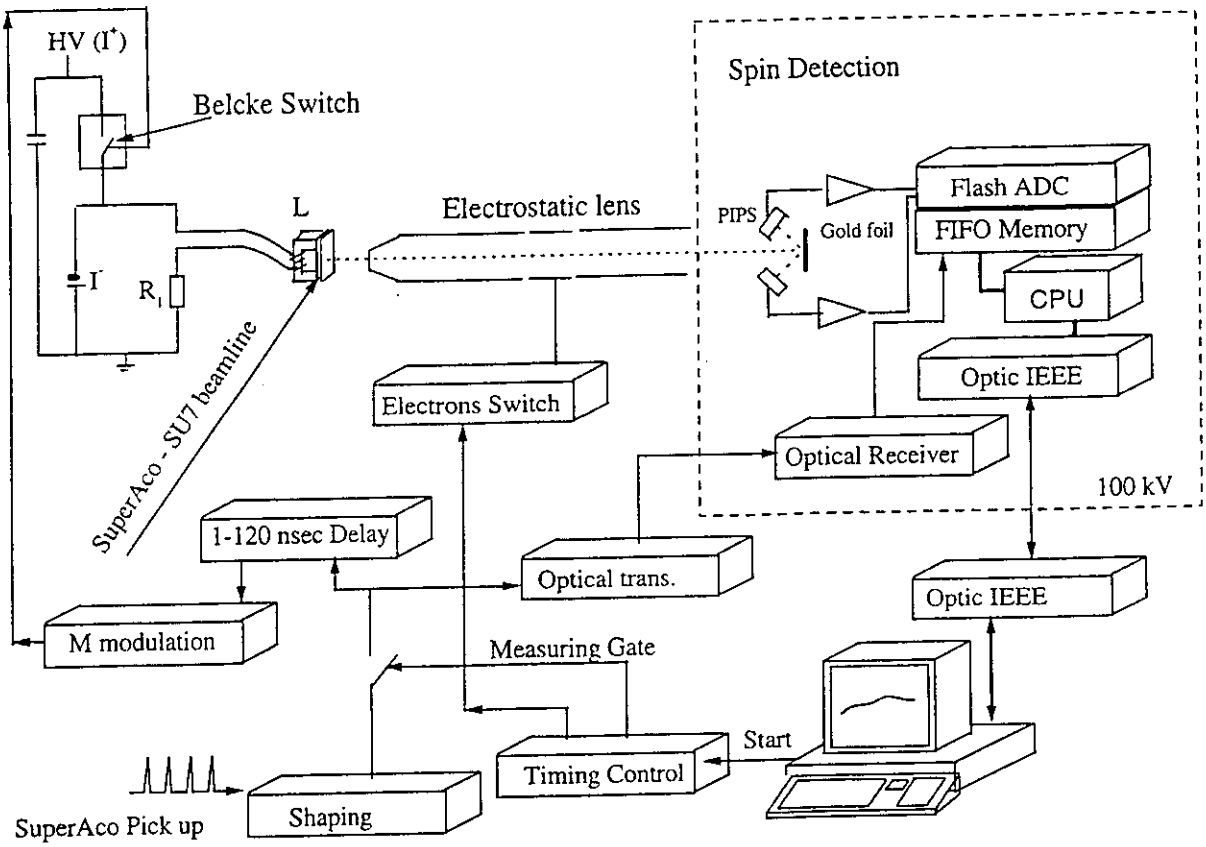

FIG. 1. Scheme of the experimental setup. Upper left: the electrical circuit for creating the magnetizing field, sample mounting, and geometry of the experiment. Right hand inset: detection electronic of the Mott detector (floating at 100 kV). Lower left: synchronization signal from the storage ring and timing control scheme.

dH/dt. The values of dH/dt obtained from our magnetizing circuit are indicated in Fig. 2 (linear approximation of the raising edge). For both kind of experiments, a measuring event corresponds to the collection and the measurement of one electrons bunch created by one light pulse.

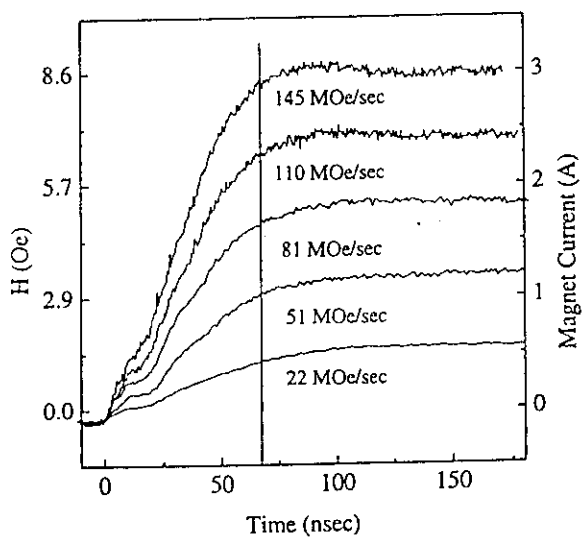

FIG. 2. Time structure of magnetizing field for different values. The applied magnetizing field reaches a constant value after 70 ns. In the linear transient regime (20 ns$<t<$60 ns) the field gradient values are indicated.

After the trigger signal, the acquisition lasts until the FIFO memory is full, i.e., after 983 μs. Whenever the apparatus is not triggered, the electron beam is deviated from the Mott detector by an electrostatic lens; this prevents the saturation effects of the solid state detectors and electronics. The time structure of such a measuring procedure is reported in Fig. 3, as given from the timing control electronics of Fig. 1. When the computer gives the start signal, the electrons switch is opened [Fig. 3(a)] and after a delay of about 2 ms (to establish stationary electrostatic conditions) the measuring gate [Fig. 3(b)] enables the transmission of the SuperAco clock signal [Fig. 3(c)]. The rise of the first clock transition triggers the current pulse in the windings producing the magnetizing field. This allows to start the sequence of measuring events with a well-defined delay with respect to the current pulse (with an incertitude smaller than one ns), i.e., to perform pump-probe type experiments. The ultimate time resolution is defined by the SR pulse duration (500 ps). The shape of the magnetic pulse, measured from the resistance R, is shown in Fig. 3(d) in the case of a magnetic field reversal produced by switching the current in the magnetic circuit from -300 mA to 3 A. Finally, the electrons switch is closed within 1 ms from the end of the acquisition and the trigger transmission is disabled. The FIFO memory is restored by a 68070 microprocessor and the system is ready for a new measuring process.

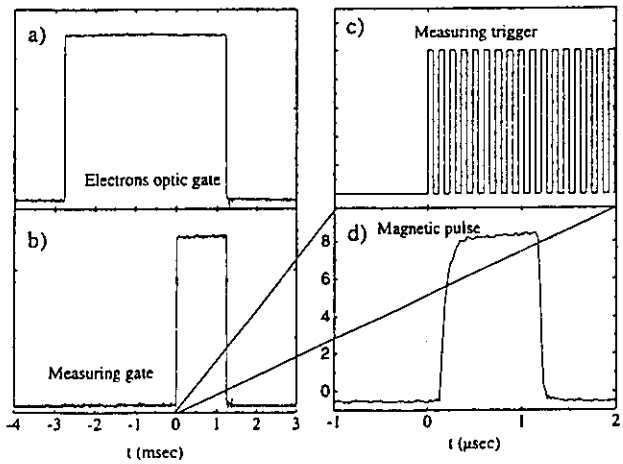

FIG. 3. Timing control of the experiment: (a) Opening of the electrons switch allowing the photoelectrons to be accelerated to the Mott detector; (b) after 2 ms the measuring gate enables the transmission of the trigger signal. (c) Trigger signal. (d) The magnetizing pulse (−300 mA to 3 A in this example).

III. RESULTS

The presence of an external magnetic field applied to the sample during the measurements affects the trajectories of the photoejected electrons; this may result in an additional, undesired, asymmetry. Test experiments demonstrated that the SP value obtained from a magnetically saturated surface is stable even in presence of magnetic pulses exceeding the saturation value. Figure 4 shows such a test for pulses of +3 A (saturation value <+50 mA). The effect of the applied field on the scattered intensities in the left and right channels

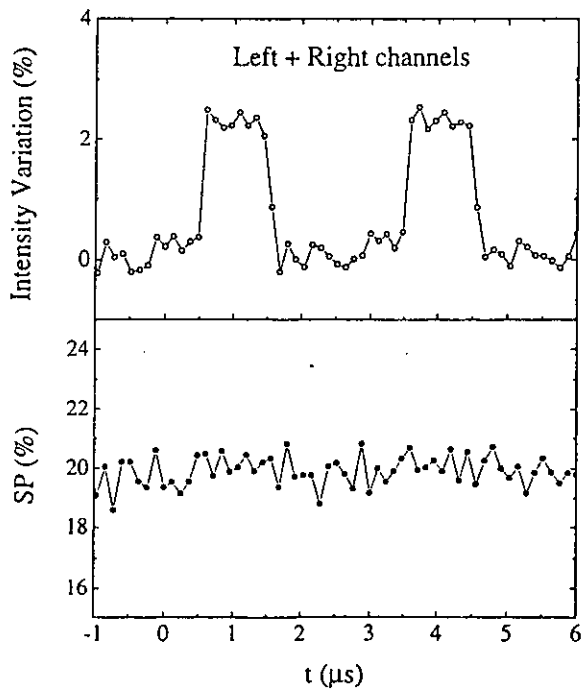

FIG. 4. Test of SP measurement with large applied fields. Top panel: variation of total count rate on detectors during H field pulses of ~9 Oe. Bottom panel: the SP measure is unaffected.

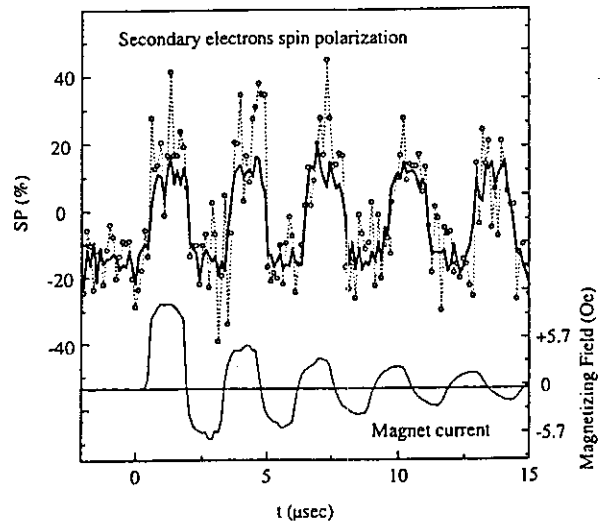

FIG. 5. Time-resolved SP measurements showing the variations of magnetization induced from the external magnetic field oscillations shown in the bottom of the figure. The values of the magnet current are reported on the y scale on the right. The sample was a 15 Å Fe layer grown on Vitrovac. Open circles correspond to an SP value in a single bunch measurements, i.e., each 120 ns. The continuous line is the average on ten measurements.

of the Mott detector is shown in the top curves of Fig. 4, and the corresponding SP is shown in the lower panel. The 2.5% variation in the intensities does not affect the SP, thus demonstrating that the SP is a genuine measure of the sample magnetization even in presence of an external field.

A. Real time measurements: Magnetization reversal dynamics

Independent SP data are collected and stored after each SR pulse therefore allowing, with a sampling frequency of 1/120 ns=8.33 MHz to follow the reversal of the surface magnetization after the application of a reversal magnetizing field pulse. As an example of the reversal dynamics as a function of applied field strength we report in Fig. 5 the SP oscillations following the application of an oscillating magnetizing field with damped magnitude. The full line at the bottom represents the current through the magnetic circuit. The open symbols represent the single-pulse SP data and the continuous thick line is the result of an average on 10 repeated measurement cycles. The SP measurement obtained with a single SR pulse is sufficient to obtain the sample magnetization. As the magnitude of the applied magnetic field is reduced the corresponding SP reversal occurs with an increasing delay. The magnetization reversal process has been studied by the application of magnetic pulses with symmetric values (from $+H$ to $-H$) to a 2 nm Fe film on Vitrovac at $T=300$ K. In Fig. 6 we show the surface sensitive SP data (average of 300 repeated measurement cycles) compared with bulk sensitive measurements obtained by an induction search coil in identical experimental conditions. The data show that the total time required for completing the reversal is of the order of some μs and strongly depends on the value of the applied field. The data also show that the magnetization reversal dynamics is different at the surface (Fe overlayer) with respect to the substrate (Vitrovac). The continuous lines through the data are obtained as best fit of a

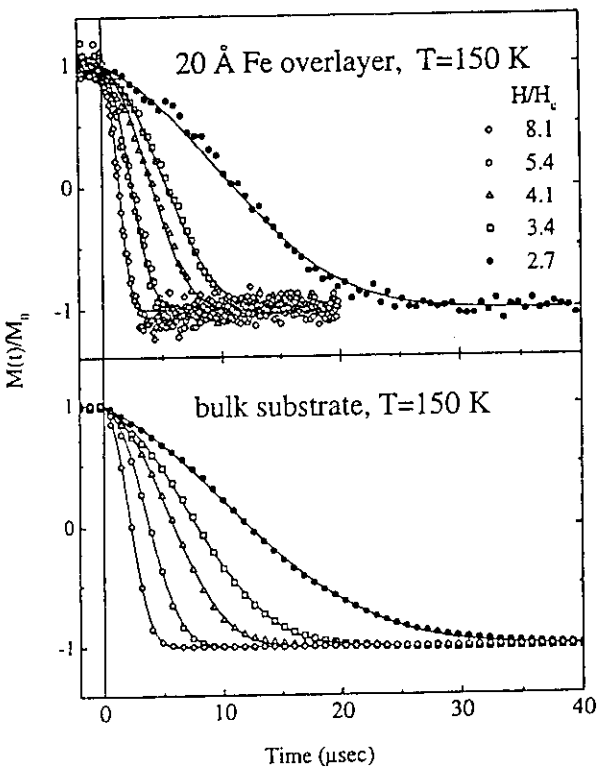

FIG. 6. Time-resolved SP measurements (average of 300 measurements) showing the magnetization reversal of a thin Fe layer (20 Å) deposited at RT on a Vitrovac ribbon. From left to right, the curves correspond to decreasing values (from 200 to 75 mA) of the symmetric square H field pulses. The magnetization value is reported as $M(t)/M_0$, where M_0 is the SP value in stationary conditions, i.e., $t=0$. At time below zero the film is magnetically saturated, i.e., in equilibrium condition. The continuous lines are the best fits obtained following the model of Ref. 15.

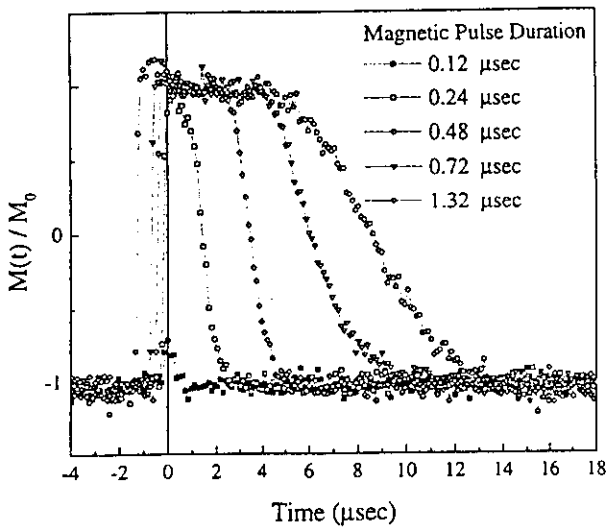

FIG. 7. Results for asymmetric $+H_1$ and $-H_2$ field pulses ($H_1=1.5$ Oe; $H_2=0.3$ Oe) as a function of different pulse duration. No magnetization reversal is observed for a 0.12 μs time. A complete magnetization reversal is observed starting from a 0.24 μs duration of applied magnetizing field.

semiempirical model of the magnetization reversal for continuous films after Labrune *et al.*[16] This model, likewise other similar models,[17,18] describes the magnetization reversal with parameters representing the probability of nucleating a magnetic domain in the applied field direction, and the speed of growth of magnetic domains. Although such class of models with activation-barrier-like parameters brings only limited insight in the reversal process, the good fit obtained to our data allows to conclude that in this time domain of excitation and dynamics the magnetization reversal of an iron ATF is governed by domain processes. The dependence of the effective coercivity on the magnitude of the applied field is well observed in this time domain.[19]

A variety of experiments can be performed by controlling the following parameters: sign, magnitude, raise time, and duration of the applied magnetic field, sample thickness, coupling to the magnetic driver substrate, sample temperature, film continuity, etc. An example for asymmetric magnetic field pulses (different values for $+H_1$ and $-H_2$) of fixed magnitude, but variable time duration is shown in Fig. 7. In the figure the zero of the time scale indicates the field inversion from $+H_1$ to $-H_2$. The duration of the $+H_1$ field pulse is seen as negative time extent of the positive magnetization state. With applied $+H_1$ fields pulses of 0.12 μs duration the surface magnetization remains basically unperturbed, but starting from 0.24 μs of $+H_1$ duration the magnetization of the surface is completely reversed. It is interesting to observe that the dynamics of the reversal process strongly depends on the duration of the high field $+H_1$ pulse, i.e., of the previous history of the sample. These experiments show the importance of surface magnetic after effects.[19,20]

B. Pump probe experiments: Fast magnetization reversal

Introducing a delay between the SR clock and the magnetic field pulses, as explained above, pump-probe experiments can be performed and the time resolution can be pushed to its limit, i.e., the SR light pulsewidth (~500 ps at SuperAco). The delay between pump (H field pulse) and probe (light pulse from the synchrotron) can be changed between each data acquisition producing reliable data sets with 1 ns resolution. The faster magnetization reversal that we could observe for a 2-nm-thick Fe film on Vitrovac was completed in a time $t\simeq 40$ ns (see Fig. 8) which corresponds to 25 MHz reversal rate. In this case the magnetization reversal time is shorter then the time needed to establish a steady current state within the applied field circuit, i.e., the magnetization change is driven by a changing applied field. In particular, for a magnetizing pulse of $H/H_C=140$ like that in Fig. 8, the complete reversal is obtained when the field has reached 60% of the final value. The pump-probe experiments with high time derivative of the applied magnetizing field H must be understood by carefully considering the actual dynamics of the H field pulse, i.e., the exact value of dH/dt across the time interval of the magnetization reversal process.[21]

IV. CONCLUSIONS AND OUTLOOK

We have here presented a new approach to the study of the dynamics of magnetization at surfaces based on the combination of SP measurements and time structure of SR. The

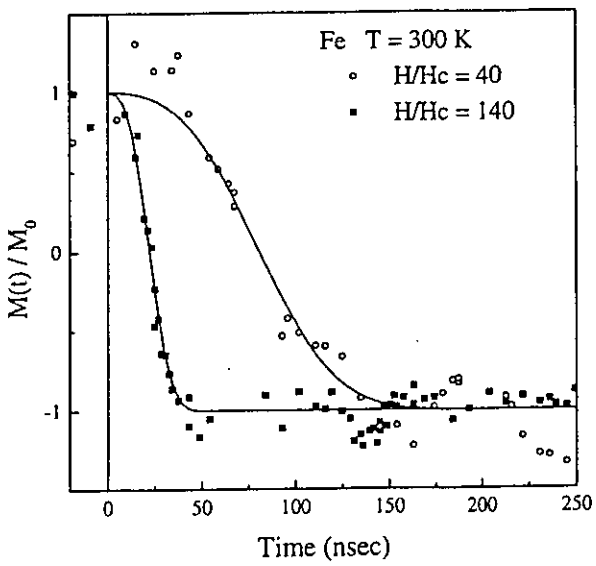

FIG. 8. $M(t)/M_0$ as a function of time, where M_0 is the SP value in stationary conditions, for a pump-probe experiment. Two kinds of magnetizing field pulses are shown: one with asymptotic values of $H/H_C = 40$ (open circles) and with gradient of 51 MOe s^{-1}. The second with an asymptotic value of $H/H_C = 140$ (filled squares) and a gradient of 145 MOe s^{-1}. The sample was a 2 nm Fe layer on Vitrovac at room temperature.

time resolution of the method is entirely set by the duration of the SR light pulse for pump-probe experiments and by the repetition rate of the SR pulses in real time experiments. In this last case the actual limiting rate of independent measurements is set by the dead time in between independently recordable signals which fact limits our current setup to a maximum real-time measurement rate of 12–15 MHz. The important aspect of our experimental setup is the intrinsic surface sensitivity of the SP measurement, which makes it the first synchrotron radiation-based time-resolved surface magnetometer. The whole domain of surface magnetic dynamics at the relevant time scales can be explored with the above-described experiments, including nonstationary states of a surface undergoing structural phase transitions. The few experimental results selected for this presentation all indicate that domain processes determine the surface magnetization reversal dynamics at ~10 MHz rate.

ACKNOWLEDGMENTS

The results presented here represent the achievement of the project, "Time Resolved Surface Magnetometry with Synchrotron Radiation," by G. Rossi and H. C. Siegmann, supported by the Swiss National Fund under Program 24. The authors gratefully acknowledge the continuous support of H. C. Siegmann and the collaboration of D. Guarisco and M. Liberati at different stages of the experimental work. G.P. acknowledges support by the EC Human Capital and Mobility Program.

[1] M. P. Sharrok, J. Appl. Phys. 76, 6413 (1994); P. J. Flanders and M. P. Sharrok, *ibid.* 62, 2981 (1987).
[2] R. H. Victora, Phys. Rev. B 63, 457 (1989).
[3] J. Pommier, P. Meyer, G. Penissard, J. Ferre P. Bruno, and D. Renaud, Phys. Rev. Lett. 65, 2054 (1990).
[4] P. J. Flanders and M. P. Sharrock, J. Appl. Phys. 62, 2918 (1987).
[5] B. Raquet, M. D. Ortega, M. Goiran, A. R. Fert, J. P. Redoules, R. Mamy, J. C. Ousset, A. Sdaq, and A. Khmou, J. Magn. Magn. Mater. 150, L5 (1995).
[6] F. B. Humphrey and E. M. Giorgy, J. Appl. Phys. 30, 935 (1959).
[7] W. D. Doyle, L. He, and P. J. Flanders, IEEE Trans. Magn. MAG-17, 3020 (1981).
[8] A. Vaterlaus, T. Beutler, and F. Meier, Phys. Rev. Lett. 67, 3314 (1991).
[9] D. Guarisco, Ph.D. thesis, ETH Zuerich, 1995.
[10] H. C. Siegmann, J. Phys.: Condens. Matter 4, 8935 (1992), and references therein.
[11] G. Rossi and F. Sirotti, in *Magnetism and Synchrotron Radiation*, ed. by E. Beaurepaire, B. Carriere, and J.-P. Kappler (Les Editions de Physique, Les Ulis, 1997), pp. 325–346.
[12] J. Kessler, *Polarized Electrons*, 2nd ed. (Springer, Berlin, 1995).
[13] H. C. Siegmann, F. Meier, M. Erbudak, and M. Landolt, Adv. Electron. Electron Phys. 62, 1 (1984).
[14] J. Kessler, Rev. Mod. Phys. 41, 3 (1969).
[15] G. Rossi, F. Sirotti, and G. Panaccione, in *Core Level Spectroscopies for Magnetic Phenomena: Theory and Experiment*, Vol. 345 of NATO-ASI Series B, edited by P. Bagus, G. Pacchioni, and F. Parmigiani (Plenum, New York, 1995), and references therein.
[16] M. Labrune, S. Andrieu, F. Rio, and P. Bernstein, J. Magn. Magn. Mater. 80, 211 (1989).
[17] P. Bruno, G. Bayreuhter, P. Beauvillain, C. Chappert, G. Lugert, D. Renard, J. P. Renard, and J. Seiden, J. Appl. Phys. 68, 5759 (1989).
[18] A. Lyberatos, J. Earl, and R. W. Chantrell, Phys. Rev. B 53, 5493 (1996).
[19] F. Sirotti and G. Rossi (unpublished).
[20] G. Bayreuter, P. Bruno, G. Lugaert, and C. Turtur, Phys. Rev. B 40, 7399 (1989).
[21] B. Raquet, R. Mamy, and J. C. Ousset, Phys. Rev. B 54, 4128 (1996).

ATOM SPECIFIC SURFACE MAGNETOMETRY WITH LINEAR MAGNETIC DICHROISM IN DIRECTIONAL PHOTOEMISSION

GIORGIO ROSSI,[1,2] FAUSTO SIROTTI,[2] and GIANCARLO PANACCIONE[2]
[1] *Laboratorium für Festkörperphysik, ETH-Zürich, CH-8093*
[2] *Laboratoire pour l'Utilisation du Rayonnement Electromagnetique, CNRS, CEA, MESR F-94305 Orsay*

ABSTRACT

A practical atom specific surface magnetometry can be based on the measure of magnetic dichroism in the angular distribution of core photoelectrons using linearly polarized synchrotron radiation. The magnetic dichroism effect on the photoemission intensity of 3p core levels of the ferromagnetic transition elements is as large as 46% in the case of Fe(100). The most efficient scheme for measuring the magnetic dichroism in photoemission requires two mirror experiments in chiral geometry, i.e. only two times more experiments than standard core level photoemission for surface chemical analysis. We describe the dichroism magnetometry and show examples for Fe, Co, Ni and Cr surfaces and interfaces, including the measurement of the temperature dependence of the Fe(100) surface magnetization and of the effect of S-segregation on the surface magnetic moment of iron.

INTRODUCTION

The understanding of the magnetic properties of surfaces and low dimensional solids requires accurate measurements of all the structural, chemical, and magnetic parameters of the surface atoms.

The field of surface magnetism has been opened when the measurement of the magnetization of surface and near-surface atoms became practical by the application of spin-polarimetry to the photoelectrons and secondary electrons ejected from surfaces.[1] The measure of spin polarization (SP) of secondaries is intrinsically surface sensitive due to the short escape depth for low energy photoelectrons in ferromagnets, and can be understood semi-quantitatively, but gives an average magnetization values, i.e. does not resolve contributions from individual atomic species constituting the magnetic surface. On the other hand the basic surface science spectroscopies, Auger electron spectroscopy and photoelectron spectroscopy, which allow a full chemical characterization and sensitivity to local order in the diffraction of the ejected electrons, are not directly sensitive to magnetism. To gain magnetic sensitivity AES and PES have been measured in the spin-resolved mode, i.e. by measuring the number of Auger electrons or core photoelectrons with their spins aligned or counteraligned to a macroscopic magnetization direction.[2-4] These are close to ideal tools for surface magnetism, but suffer for a great technical handicap: the low efficiency of spin-detection which is only some 10^{-3} and severely reduces the applications of these techniques. An alternative is to exploit the fact that polarized atoms, like the atoms in a magnetically ordered ferromagnetic material, can be recognized by their directional anisotropies in the photoionization matrix elements.

Angular photoemission experiments on core levels about the magnetization direction (vector) show dichroism and therefore allow to probe magnetism in a highly efficient way. A large magnetic dichroism effect is shown in figure 1 for the Fe 3p core levels from Fe(100). The

Mat. Res. Soc. Symp. Proc. Vol. 384 © 1995 Materials Research Society

dichroism is obtained as the differences of two photoelectron spectra of the exchange splitted Fe 3p magnetic sublevels, measured in the mirror chiral geometries which are shown in the inset of the figure 1, using linearly polarized synchrotron radiation at soft X-ray energies. This effect was observed first by Roth and coworkers.[5] The special case of magnetic dichroism in photoemission which is measured as a difference in the angular distribution of photoelectrons between two mirror experiments, is called linear magnetic dichroism in the angular distribution of photoelectrons (LMDAD).[7–11] We show below that a practical surface magnetometry can be based on the LMDAD effect, combining all the power of photoelectron spectroscopy with magnetometric information at a total cost of doubling the experimental effort of a standard core level photoemission surface analysis.

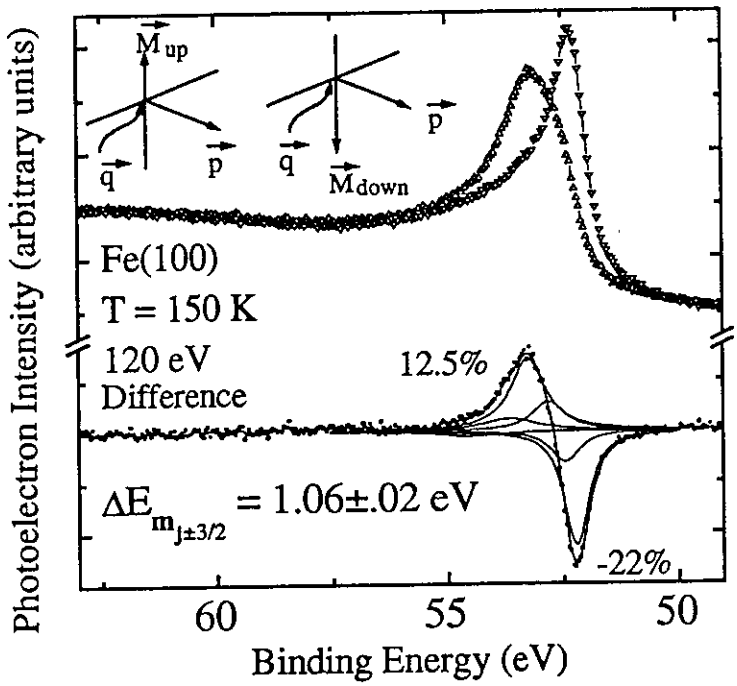

Fig.1: Fe 3p photoemission mirror experiments done in the chiral geometries shown at the top, and the LMDAD dichroism curve for Fe(100). The dichroism is fitted by a sextuplet of magnetic sublevels which are weighted by the angular matrix elements.[ref. 8] The extrema of the LMDAD curvve coincide with the mj=+-3/2 sublevels.

PRINCIPLES

In a core level photoemission experiment of a ferromagnetic material the photoexcited core hole state of total angular momentum J is split by the spin orbit and exchange interactions with the spin polarized valence electrons into sublevels with a given projection m_j on the magnetic quantization axis. Exchange dominates over orbital interaction and $J = L + S$ is not a good quantum number so that the ordering of the m_j sublevels is different with respect to the Zeeman effect. By disregarding altogether the manybody processes involved in the photoemission from atoms and from solids, as well as the possible splitting of the high energy final states, one expects each m_j sublevel to contribute intensity with a characteristic angular distribution.[12] Within this one-electron atomic picture the intensity and the angular distribution of the photoemission spectrum is completely determined by the core hole multiplet. The angular dependence of photoionization of a particular m_j core sublevel can be measured if the energy splitting of the core hole is at least of comparable size with

respect to the intrinsic width of the core hole. The relative variations of lineshape measured in the mirror experiments of figure 1 represent the relative variations of intensity from a grid of effective m_j sublevels for the Fe 3p core hole.[8,11] The experimental variations can be compared with calculated photoionization cross sections.[12,13,10]

LMDAD experiments on Fe, Co, Ni and Cr 3p photoemission.

The experimental LMDAD spectra for the ferromagnetic transition metals and for chromium (layered antiferromagnet) measured at 150 K are collected in figure 2. The top curves in each panel represent the as measured spectra at the indicated photon energies. Up full triangles indicate the spectra measured with the external magnetic field direction in the up-vertical direction, and open down-oriented triangle indicate the experimental points measured after reversal of the surface magnetization, by the external field directed in the down-vertical direction. The chiral geometry is the same for all the experiments but the angular acceptance of the analyzer is different in the case of Fe at 170 eV. The second panel represents the spectra after background substraction (integral background plus exponential decay of secondaries). This procedure allows to estimate the amount of photoemission intensity at final state energies lower than the main 3p peak, i.e. the deviation from the simple one-electron reference model.[11] Finally the bottom panels show the experimental difference curves i.e. the LMDAD spectra. The photoemission magnetic asymmetry is defined as $A = \frac{I_{up} - I_{down}}{I_{up} + I_{down}}$, where $I_{up\ (down)}$ are the photoelectron spectral intensities obtained with the magnetization in the upward (up) or downward ($down$) directions.

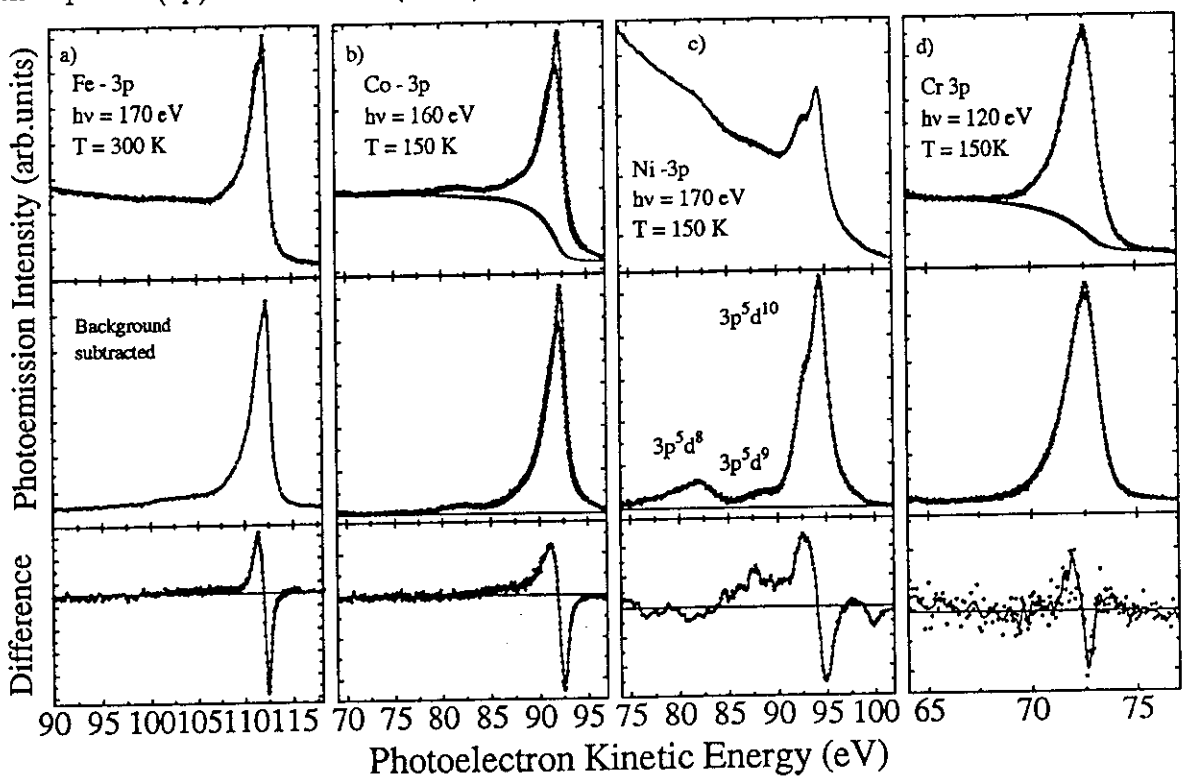

Fig.2: 3p LMDAD spectra of Fe, Co, and N polycrystalline layers, and of the Cr(100) surface.

The maximum LMDAD asymmetry was 46% of the Fe 3p intensity (corresponding to a 22% variation of the total photoemission including background) measured at $140K$ and for $h\upsilon = 120eV$ for a clean Fe(100) surface.

The three ferromagnetic 3d metals all show similar dichroism curves under the main peak, with the magnitude of the asymmetry scaling with the element and with the photon energy. The LMDAD asymmetry result are related to the magnetic moment of the metals, but in a complex way. By inspecting the spectra one finds that the photoemission intensity is basically all concentrated under the main peak in the case of Fe 3p, but it shows tails and well resolved satellites in the cases of Co and Ni. This is a consequence of the increasing correlation of the d-bands with d-filling, which implies a higher probability of multiplet final state configurations. The Ni 3p peak and satellites correspond to $3p^5d^{10}$, $3p^5d^9$ and $3p^5d^8$ final state configurations respectively. The photoemission intensity of the satellites amounts to 20% of the total intensity in nickel. Since every configuration is different, it will display in principle a different magnetic dichroism. Such result was previously suggested by a circular dichroism experiment on Ni.[14] In the 4th panel we see the Cr 3p photoemission spectra from an epitaxial overlayer on Fe(100). The ferromagnetic order of the Cr surface can be seen by the presence of a LMDAD curve. Its orientation with respect to the substrate Fe can be directly observed from the sign of the LMDAD curve (reversed in this case indicating antiferromagnetic coupling of the Cr surface to the substrate).

LMDAD as a Kerr-like diagnostic tool

A direct application of LMDAD is to probe the magnetic order at surfaces in a similar qualitative way as the magneto-optic Kerr effect probes the bulk magnetic order, but with the important advantage of chemical sensitivity.

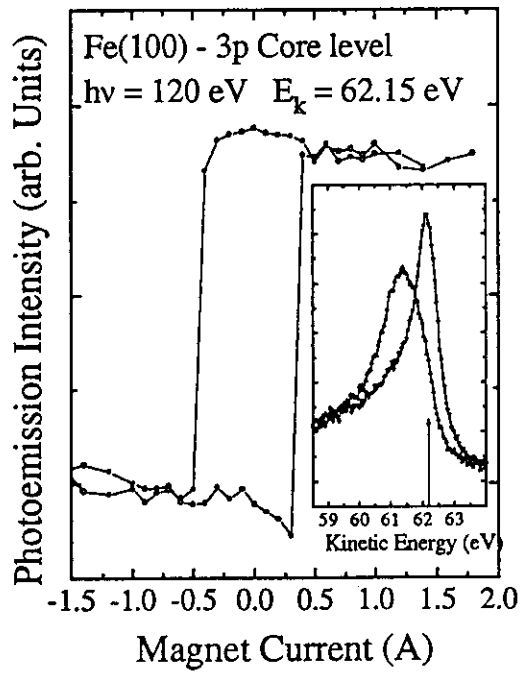

Fig.3: Magnetic hysteresis loop measured with LMDAD on Fe(100).

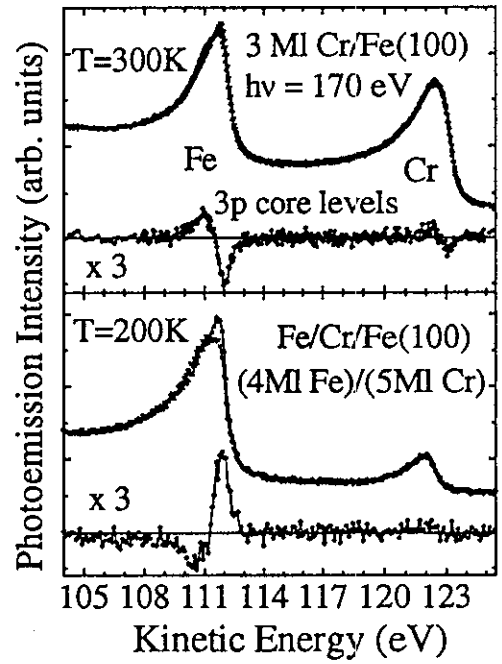

Fig.4: LMDAD spectra for the Cr/Fe(100) interface and Fe/Cr/Fe(100) trilayer.

Figure 3 shows the LMDAD spectra at two stages during the growth of a Fe/Cr/Fe trilayer structure. The top panel shows that the ferromagnetic order of the Fe(100) substrate is not

disturbed by the epitaxial growth of 3 ML of Cr. The Cr 3p also shows LMDAD indicating ferromagnetic order in plane. Cr is known to grow along the [100] direction as a layered antiferromagnet,[15] the measured Cr 3p LMDAD is due to the uncompensated signal from the surface layer. The lower panel shows the completion of the trilayer structure by epitaxial overgrowth of Fe on a 5 ML thick Cr interlayer. The LMDAD signal shows that the top Fe film is antiferromagnetically coupled to the substrate iron across the 5 monolayers of chromium.

The LMDAD asymmetry can be measured at the optimum final state energy (i.e. where the asymmetry is maximum) while varying the external magnetic field to obtain magnetic hysteresis curves for the selected atoms. A LMDAD magnetic hysteresis curve for Fe(100) is shown in figure 3. There is a practical limitation of photoemission hysteresis curves which is due to the quite small value of external field that can be present *during* the photoemission measurement.

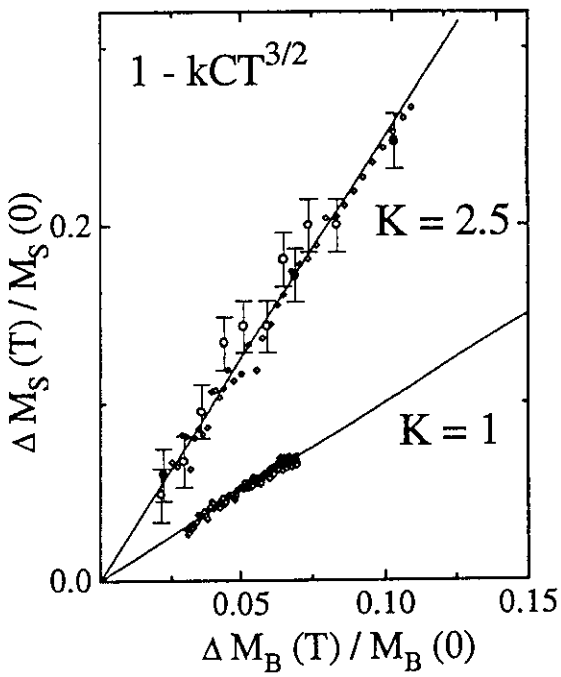

Fig.5: Thermal decrease of the relative surface magnetization as measured by Fe 3p LMDAD asymmetry.

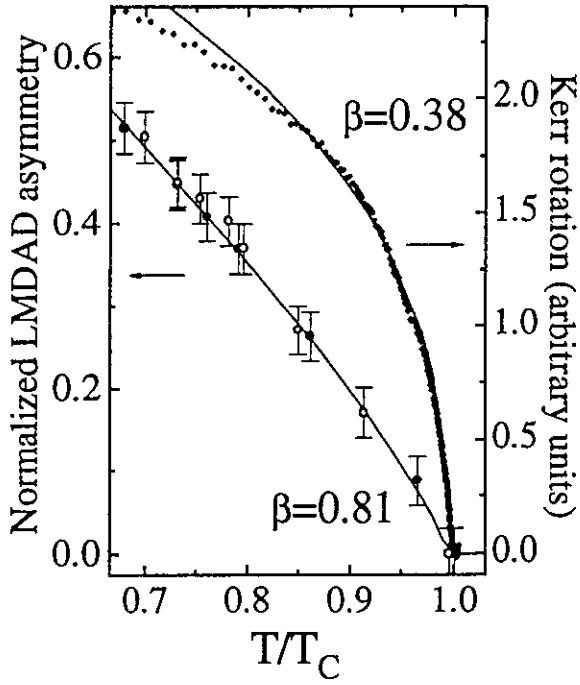

Fig.6: LMDAD (circles) and Kerr rotation (diamonds) as afunction of reduced temperaturein the near Tc region..

Testing the Temperature Dependence of LMDAD in The Spin Wave Regime and Near T_{Curie}.

The temperature dependence of the surface magnetization in the spin wave regime has been measured for Fe-Ni-B and for Fe layers and interfaces in SP experiments. The results indicate that the exchange interaction within the surface and along a path perpendicular to the surface are different from the bulk exchange, and can be obtained by fitting model calculations to the slope of the $M_S(T)$ curve.

A crucial test for the LMDAD photoemission magnetometry is the dependence of the LMDAD asymmetry on temperature for a clean Fe(100) surface, and to compare the results

with spin polarization (SP) measurements. The temperature dependent results of the Fe 3p LMDAD asymmetry, SP of the secondary electrons as measured with a 100KV Mott-scattering experiment, and of bulk magnetization sensitive Kerr rotation data are shown in figures 4 and 5.[16]

For $T \leq .4T_C$, the thermal decrease of the relative surface magnetization $\Delta M_S(T)/M_S(0)$ of atomically clean Fe(100) is consistently measured by LMDAD and by SP. The results are described by the law $M(T)/M(0) = 1 - kCT^{3/2}$ of spin-wave theory.[17] The Kerr data measure the bulk thermal decrease of relative magnetization with $k = 1$ which determines the bulk constant C. A surface enhancement factor $k \simeq 2.5$ is obtained by fitting the LMDAD and SP data to the $T^{3/2}$ law: it represents the reduction of the exchange interaction of the Fe(100) surface atoms along a path perpendicular to the surface.[18] In the critical region (figure 3) the Kerr-rotation and LMDAD signals vanish with, respectively, bulk and surface critical exponents according to $M_B \propto (1 - T/T_{CB})^{\beta_B}$ and $M_S \propto (1 - T/T_{CB})^{\beta_S}$.[19] The Fe 3p LMDAD results for Fe(100) are described by a surface critical exponent $\beta_S = 0.81 \pm 0.01$, to be compared with $\beta_B = 0.38 \pm 0.01$ from Kerr rotation. The LMDAD results agree with previous SP measurements of energy selected secondary electrons on Fe (110),[20] and with spin-dependent elastic electron scattering results for Ni(100) and Ni(110) surfaces,[21] and are consistent with a ferromagnetic surface weakly coupled to the bulk. These results provide direct experimental proofs that the measure of photoemission magnetic dichroism gives directly the order parameter of magnetization for the Fe surface atoms $< M_S >$.

Fe 3p Fine Structure: Exchange and Spin-Orbit Parameters, Magnetochemical Shifts

From the fine structure of the 3p core levels one can evaluate the exchange splitting of the core hole. The width of the $J = 3/2$ multiplet is found here to be $1.06 \pm .02eV$ for Fe 3p. The spin orbit splitting of the 3p core holes in Fe is known from silicide data[22] to be $1.05 \pm .05eV$. The splitting between adjacent m_j sublevels corresponds to a value of exchange field of 3.5 10^7Gauss for the 3p core hole in *bcc*-Fe. This analysis is rather direct in the case of Fe 3p since the extrema of the asymmetry curve coincide with the $m_j = \pm 3/2$ sublevels, which are pure spin-orbit states and display the largest magnetic asymmetry. The "width" of the Fe 3p dichroism spectrum is therefore a direct measure of the atomic exchange interaction for the 3p core hole.

The atomic exchange depends upon the details of the spin-polarized electron states of the valence band which is determined by crystal structure and chemistry at the surface. We compare in figure 6 the 3p dichroism spectra of clean Fe(100) and S segregated Fe(100). Sulfur segregation occurs at temperatures higher then 500 C and saturates when an ordered c(2x2) superstructure is completed (clearly observed in LEED) for annealing above 600 C.[23] The 3p LMDAD dichroism spectra of Fe(100) and c(2x2)S/Fe(100) at 300K are shown in figure 4. The narrowing of the Fe 3p dichroism spectrum for the sulfurated surface shows that the $m_j = \pm 3/2$ splitting is reduced to $.99 \pm .01eV$. This indicates the at the magnetic moment of the Fe atoms bonded to the S is reduced by a large amount. The photoemission measurement averages the information of the top three layers of material , so if the reduction of magnetic moment is only occurring at Fe surface sites, this reduction is of the order of 20%. From the inspection of the magnetization dependent spectra one observes a clear "magnetochemical shift" of the peak dominated by the (minority spin) $m_j = +3/2$ sublevel when sulfur is present at the surface. The reduced magnetic moment of the Fe(100) surface and subsurface atoms when S atoms occupy the fourfold surface sites corresponding to the

c(2x2) superstructure can be attributed to hybridization of the Fe 3d bands with the S sp valence electrons.[24] This fact has implications on the valence configuration of the c(2x2) S atoms. In figure 7 we show the LMDAD spectra for the S 2p core level for the segregated c(2x2)S surface of Fe(100): the presence of dichroism shows that bonding with Fe implies a transfer of magnetic moment on the sulfur. The $m_j = \pm 3/2$ splitting of the S 2p 3/2 peak is $.45 \pm .03eV$.

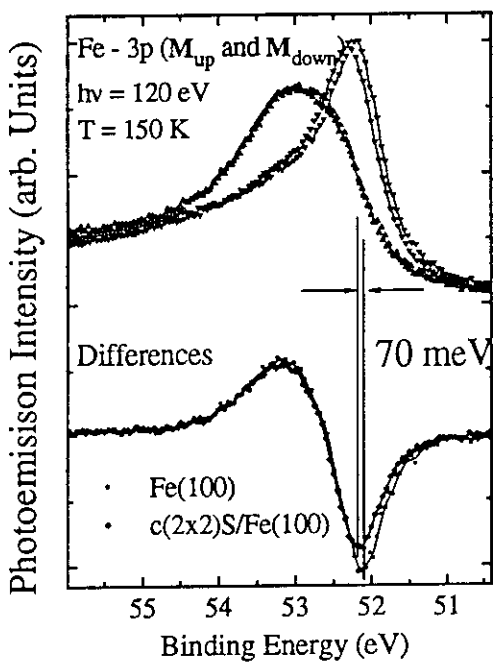

Fig.7: Fe 3p LMDAD spectra for Fe(100) and c(2x2)S/Fe(100) surface. The reduce width of the dichroism spectrum reflects the reduced magnetic splitting of the core hole.

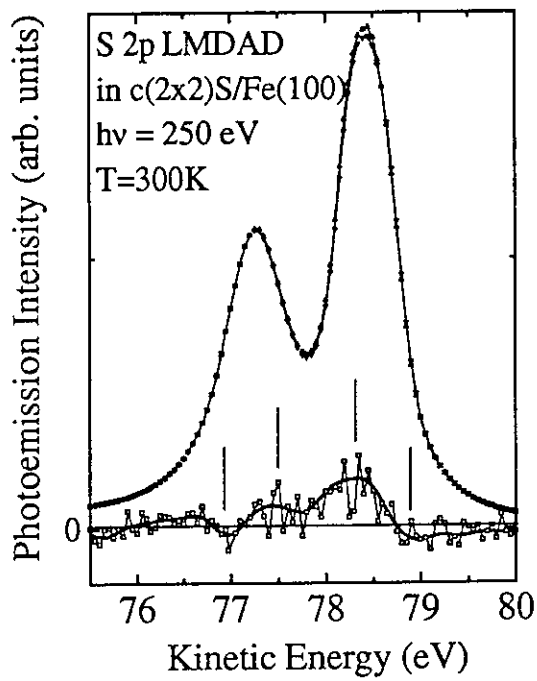

Fig.8: S 2p LMDAD spectra measured. The dichroism indicated that a magnetic moment is present on the S atoms.

A large magnetochemical shift can be measured in chromium at the interface with iron. The first epitaxial layer of Cr on Fe(100) is ferromagnetically ordered and antiferromagnetically coupled to the iron substrate. The LMDAD spectrum measured at 150 K for one monolayer (identical spectra were measured for half monolayer) of Cr on Fe(100) is shown in figure 8 and compared with the LMDAD spectrum measured from the surface of a thicker epitaxial layer. The width of the interface LMDAD spectrum is 30% larger then the width of the Cr(100) surface LMDAD for the epitaxial (100) film. The relationship between the magnetic splitting of the Cr 3p core level in the two cases, shows the relative values of the magnetic moment of chromium atoms at the interface with iron, or at the Cr(100) surface.

CONCLUSIONS AND OUTLOOK

LMDAD in chiral photoemission experiments on $l > 0$ initial states is a large effect. The measure of LMDAD on core levels is a diagnostic of ferromagnetic order which cost only a double effort with respect to the standard photoemission lineshape inspection. It is clear that photoemission magnetic dichroism provides a powerful magnetometer. The

measure of the order parameter $< M >$ is directly obtained from the asymmetry. Relative changes in the magnetic moment as a function of the atomic environment can be obtained from the LMDAD spectral widths. All the advantages of surface sensitivity and chemical sensitivity of the photoemission technique are transferred to the dichroism magnetometry. The surface analysis of ferromagnetic alloys, heterostructures, impurity terminated surfaces can be done with the full power of core level spectroscopy and magnetic order sensitivity. The fact that only two times more measurements are needed in photoemission LMDAD experiments with respect to standard photoemission, implies that the technique does not suffer for the intensity limitations which severely affects spin-resolved photoemission and even circular polarization dichroism photoemission measurements.[25,26] This implies that all the high resolution implementation of the photoemission technique made possible by new linearly polarized synchrotron radiation sources can be extended to LMDAD-magnetometry, including high energy resolution, lateral resolution, time resolution.

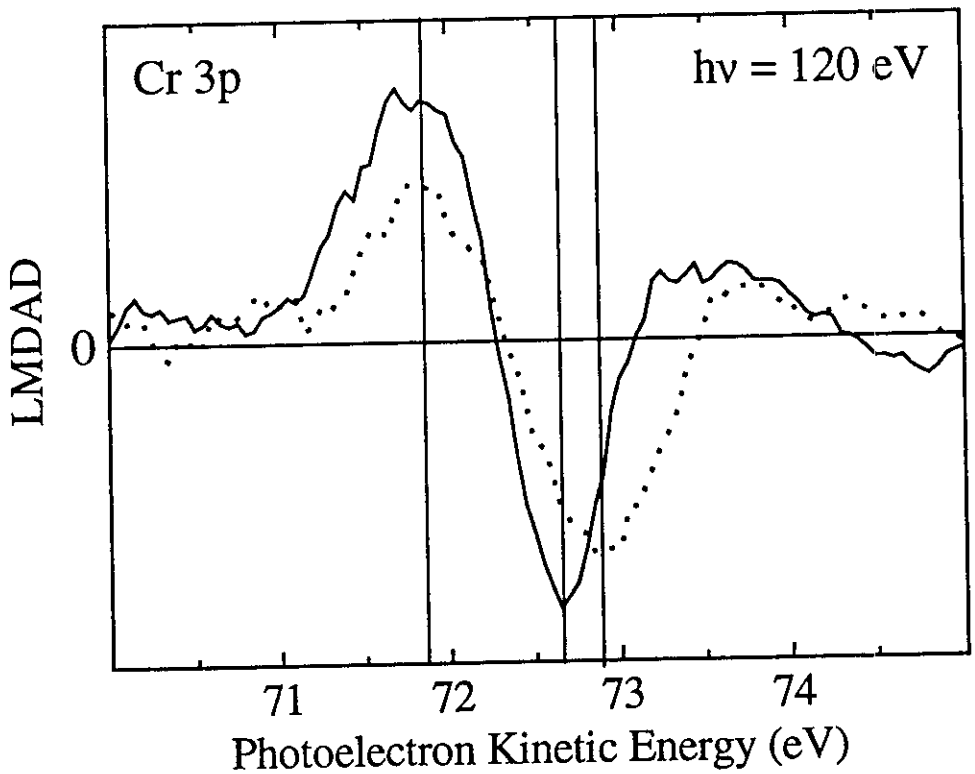

Fig.9: Cr 3p LMDAD for interface Cr atoms on Fe(100), and for the surface of an epitaxial Cr(100) film.

This work was partially supported by the Swiss National Fund for Research, under program 24. We are in debt with N.A. Cherepkov and F. Combet Farnoux for their collaboration, and to H.C. Siegmann for stimulating comments and continuous support. One of us, G.P. acknowledges the EC for a grant under the Human Capital and Mobility Program.

References

[1]H.C. Siegmann; J. Phys.: Conden. Matter **4**, 8395 (1992) and references quoted therein

[2]M. Landolt, in *Polarized Electrons in Surface Physics*, ed. by R. Feder, World Scientific, Singapore, 1985; R. Allenspach, D. Mauri, M. Taborelli, and M. Landolt, Phys. Rev. **B35**, 4801 (1987)

[3]C. Carbone, and E. Kisker; Solid State Commun. **65**, 1107 (1988)

[4]E. Kisker, in *Polarized Electrons in Surface Physics*, ed. by R. Feder, World Scientific, Singapore, 1985

[5]Ch. Roth, F.U. Hillebrecht, H. Rose, and E. Kisker, Phys. Rev. Lett. **70**, 3479 (1993)

[6]Ch. Roth, H. Rose, F.U. Hillebrecht, and E. Kisker, Solid State Commun. **86**, 647 (1993)

[7]F. Sirotti and G. Rossi, Phys. Rev. **B49**, 15682 (1994)

[8]G. Rossi, F. Sirotti, N.A. Cherepkov, F. Combet Farnoux, and G. Panaccione, Solid State Commun. **90**, 557 (1994)

[9] D. Venus; Phys. Rev. **B48**, 6144 (1993), ibid. **49**, 8821 (1994))

[10]G. van der Laan; Phys. Rev. **B51**, 240 (1995)

[11]G. Rossi, F. Sirotti and G. Panaccione; in *Core Level Spectroscopies For Magnetic Phenomena: Theory and Experiment* ed. by P.S. Bagus, G. Pacchioni, and F. Parmigiuani, Plenum ASI-NATO series 1995.

[12]N.A. Cherepkov, Phys. Rev. **B50**, 13813 (1994)

[13]E. Tamura, G.D. Waddill, J.G. Tobin, and P.A. Sterne; Phys. Rev. Lett. **73**, 1533 (1994)

[14]G. van der Laan, M.A. Hoyland, M. Surman, C.F. J. Flipse, and B.T. Thole, Phys. Rev. Lett **69**, 3827 (1993)

[15]J. Unguris, R.J. Celotta, and D. Pierce, Phys. Rev. Lett. **69**, 1125 (1992)

[16]F. Sirotti, G. Panaccione, and G. Rossi, to be published.

[17]J. Mathon and S.B. Ahmad, Phys. Rev. **B37**, 660 (1988).

[18]D. Mauri, D. Scholl, H.C. Siegmann, and E. Kay; Phys. Rev. Lett. **61**, 758 (1988); D. Scholl. M.Donath, D. Mauri, E. Kay, J. Mathon, R.B. Muniz, H.C. Siegmann; Phys. Rev.**B43**, 13309 (1991)

[19]K. Binder, in *Phase Transitions and Critical Phenomena* vol 8, ed C. Domb and J. Lebowitz (New York, Academic)

[20]M. Taborelli, O. Paul, O. Zuger, and M. Landolt; Journal de Physique **49**, C8-1659 (1988).

[21]S.F. Alvarado, M. Campagna, and H. Hopster, Phys. Rev. Lett. **48**, 51 (1982)

[22]F. Sirotti, M. De Santis, and G. Rossi, Phys. Rev. **B48**, 8299 (1993)

[23]K.O. Legg, F. Jona, D.W. Jepsen, and P.M. Marcus; Surf. Sci. **66**, 25 (1977).

[24]S.R. Chubb, and W.E. Pickett; Phys. Rev. **B38**, 10227 (1988).

[25]L. Baumgarten, C.M. Schneider, H. Petersen, F. Schafers, and J. Kirschner; Phys. Rev. Letters **65**, 492 (1990)

[26]H. Ebert, L. Baumgarten, C.M. Schneider, and J. Kirschner, Phys. Rev.B **44**, 4406 (1991)

Magnetism of atomically thin fcc Fe overlayers on an expanded fcc lattice: $Cu_{84}Al_{16}(100)$

Waldemar A. A. Macedo
Laboratório de Física Aplicada, Centro de Desenvolvimento da Tecnologia Nuclear, CNEN, 31270-010 Belo Horizonte, Brazil

Fausto Sirotti and Giancarlo Panaccione
Laboratoire pour l'Utilisation du Rayonnement Electromagnetique, CNRS, CEA, MESR, F-94305 Orsay, France

Axel Schatz* and Werner Keune
Laboratorium für Angewandte Physik, Gerhard-Mercator-Universität Duisburg, D47048 Duisburg, Germany

Wagner N. Rodrigues
Departamento de Física, ICEX, Universidade Federal de Minas Gerais, Belo Horizonte, Brazil

Giorgio Rossi
INFM, Dipartimento di Fisica dell' Università di Modena, I-41100 Modena, Italy
and Laboratorium für Festkörperphysik, ETH-Zürich, CH-8093, Switzerland
(Received 20 October 1997; revised manuscript received 6 April 1998)

We present experimental data on the magnetic properties of atomically thin fcc (γ-phase) Fe films (1–6 atomic layer nominal thickness) epitaxially grown on $Cu_{84}Al_{16}(100)$ obtained by linear magnetic dichroism in the angular distribution of Fe $3p$ core photoelectrons excited by linearly polarized synchrotron radiation. The sign and magnitude of the Fe $3p$ photoemission magnetic asymmetry indicates the onset of in-plane ferromagnetism at 2.5(2) monolayer (ML) thickness of γ-Fe. The Curie temperature is 288(2) K for 4 ML thickness. The magnetic splitting of the Fe $3p$ mj core hole sublevels is 1.10(2) eV, i.e., the same value as measured for a bcc-Fe(100) surface where large surface and near-surface enhanced moments contribute. These results characterize the epitaxial γ-Fe on $Cu_{84}Al_{16}(100)$ as a high-spin ferromagnet for thickness up to 4 ML, with an average magnetic moment per iron atom of $2.5(1)\mu_B$. A phase transition occurs between 4 and 5 ML thickness: the magnetic order of the pseudomorphic γ-Fe film decreases consistently with the breaking into two phases with the deeper layers in a low-spin and/or antiferromagnetic phase and surface restricted ferromagnetism, similar to the case of γ-Fe/Cu(100). [S0163-1829(98)09833-6]

INTRODUCTION

Achieving an understanding of the properties and behavior of artificial nanostructures obtained by epitaxial growth and other new techniques in the search for unusual properties of materials is one of the dominant trends in physics and materials science nowadays. For magnetic materials, the search for correlation between structure and magnetic properties of metastable phases of transition metals and other nonconventional materials is particularly interesting. Among these metastable phases, fcc Fe (γ-Fe) has attracted much attention from theoretical and experimental groups. The relevance of this fact lies in the possibility of studying the magnetic properties of iron in metastable phases where it is expected that magnetovolume effects determine the ground-state configuration.[1–3] Theoretical calculations of the ground-state of bulk γ-Fe predict a nonmagnetic phase, an antiferromagnetic phase, and two ferromagnetic phases, one with a small magnetic moment of $1.1\mu_B$, and one with a high magnetic moment of $2.5\mu_B$ per atom.[1–3] The lattice parameter, i.e., the volume available for the iron atoms, determines the ground state of γ-Fe and a magnetovolume instability is predicted at 3.66 Å lattice spacing (or 12.25 Å^3 volume) inducing a first-order phase transition from the antiferromagnetic and low-spin phases to the ferromagnetic high-spin state.[1–3] Moreover, within the low-spin and in the high-spin states, the fcc Fe magnetic moment is predicted to increase monotonically with increasing lattice spacing.[1–4] Experimentally, bulk fcc Fe is stable only at elevated temperatures (>910 °C) as a paramagnetic metal and can be stabilized at lower temperatures as coherent precipitates in Cu and CuAl matrixes[5,6] or by epitaxy onto suitable fcc substrates.[7–17] Cu has a lattice parameter of 3.61 Å and therefore a volume per atom of 11.76 Å^3 that would correspond to a γ-Fe antiferromagnetic or low-spin phase.[1] Ferromagnetic order of γ-Fe was observed first for films grown by electrolytic methods on Cu(110) (Ref. 8) and for ultrathin films grown by molecular-beam epitaxy (MBE) methods on Cu(111). The experimental evidence of the stabilization of the high-spin phase, with a measured moment of $2.6\mu_B$, was obtained for γ-Fe as grown on CuAu substrates.[11] The growth of γ-Fe on Cu(100) is in fact pseudomorphic: an expansion of the lattice perpendicular to the surface can lead the system to the magnetovolume instability. The complexity of the experimental results obtained on Fe/Cu(100) is understood as a consequence of the exact structure taken by the γ-Fe as a function of thickness, deposition temperature, and interdiffusion with the substrate. A complex correspondence of magnetism and structure has been recently established.[18–28] Nondistorted fcc Fe/Cu(100) shows antifer-

romagnetic order, while an expansion of the Fe lattice perpendicular to the surface can lead to "fcc-like" Fe in the ferromagnetic state.[19–26]

In this paper we present surface sensitive magnetometric results obtained on epitaxial ultrathin Fe films grown on $Cu_{84}Al_{16}(100)$, a fcc substrate chosen in order to favor the stabilization of the "high spin" phase of γ-Fe since it has a lattice parameter 1% larger than pure fcc-Cu and therefore a 12.15 $Å^3$ volume, tuned to that predicted for the high-spin fcc Fe. The magnetism of the fcc iron epitaxial layers has been probed by linear magnetic dichroism in the angular distribution of photoelectron intensity (LMDAD) of the Fe $3p$ core levels. This novel method[29–32] allows us to analyze, in a fairly independent way,[33,34] the *magnetic order* of the fcc iron surfaces via the *magnitude* of the LMDAD asymmetry, and the relative changes of the *local magnetic moment* of the Fe atoms via the changes of the *energy splitting* of the magnetic sublevels of the Fe $3p$core hole. This is a photoelectron spectroscopy experiment: the magnetic information that is derived is an average of the contributions of the top layers, weighted by the photoelectron escape depth.

EXPERIMENT

Epitaxial Fe overlayers (1 to 6 ML thick) were grown under MBE conditions by e-beam evaporation of a high-purity Fe wire ($5N$) onto a clean surface of a $Cu_{84}Al_{16}(100)$ single crystal that presents a lattice parameter of 3.65 Å, as determined by x-ray diffraction. Both growth and measurements were performed in an ultrahigh vacuum system with a base pressure of 1×10^{-10} mbar connected to the SU7 undulator beam line at the SuperAco storage ring at Orsay. The energy of the linearly polarized undulator radiation was selected at 170 eV in order to obtain Fe $3p$ photoelectrons with kinetic energies such to give a minimum probing depth $\lambda=5(1)$ Å. This means that about 30% of the photoemission intensity originates from the surface and that the subsurface contributions are weighted by $e^{-d/\lambda}$, where d is the distance of the deeper layer from the vacuum interface. The $Cu_{84}Al_{16}(100)$ surface was cleaned by cycles of Ar^+ sputtering and annealing. Reproducible results were obtained for 30 min Ar^+ sputtering at 1.5 kV at room temperature (RT) followed by 20 min annealing at 650 K: sharp $p(1\times1)$ low-energy electron diffraction (LEED) patterns for 75 eV primary electrons were obtained. No traces of C were measured, but a small oxide signal on the Al $2p$ core level photoemission peak indicated the presence of some oxidized aluminum at the surface. The Fe evaporation rate was 0.3 Å/min, as determined by a calibrated quartz oscillator, and the residual gas pressure during the Fe evaporation was always better than 8×10^{-10} mBar. Two growth conditions were explored: the $Cu_{84}Al_{16}$ substrate was held at RT and at 150 K during iron deposition. The magnetic measurements were done by LMDAD using the same experimental setup and chiral geometry as described elsewhere.[35]

We have measured the Fe $3p$ core level from the Fe monolayers and mirror experiments were achieved by aligning the in-plane magnetization of the Fe surface via an external field up or down along the vertical direction, perpendicular to the scattering plane. The magnetic (LMDAD) asymmetry is defined as A_{LMDAD} $=[(I_{up}-I_{down}/I_{up}+I_{down})]$, where $I_{up}(I_{down})$ were the photoelectron spectral intensities obtained with the sample magnetization in the upward (up) or downward ($down$) directions. In this geometry A_{LMDAD} is nonzero only if the surface magnetization has a sizable in-plane component. The sample position and the photon energy were kept fixed in order to avoid photoelectron diffraction effects.[36]

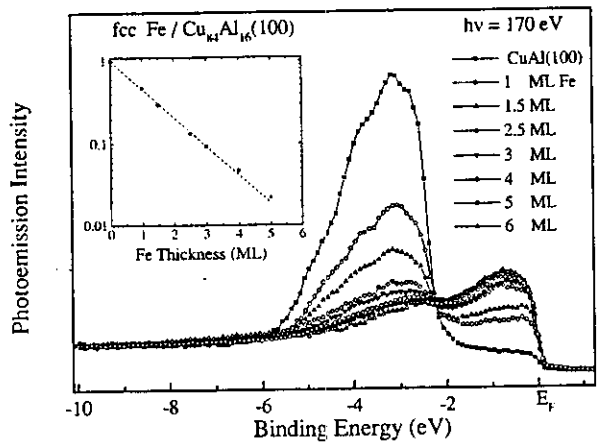

FIG. 1. SR-PES valence band spectra as a function of the Fe coverage, for the $Fe/Cu_{84}Al_{16}(100)$ system. Inset: valence band intensity decay. The result of the fitting in the inset indicates a layer-by-layer growth of the Fe films.

RESULTS AND DISCUSSION

The epitaxial growth of ultrathin Fe layers on the $Cu_{84}Al_{16}(100)$ surface at RT and 150 K was confirmed by LEED. The LEED patterns from the Fe films showed a sharp $p(1\times1)$ structure for RT growth and the same pattern with somewhat broadened spots for growth at 150 K with the same spacing as the fcc substrate. Samples grown at RT exhibited Al diffusion from the substrate through the Fe overlayers. These samples did not show magnetic dichroism either at RT or after cooling down to 150 K. The low-temperature grown films were magnetically ordered and no interdiffusion was observed within the time of the experiments. We restrict the analysis and discussion to the magnetic γ-Fe layers grown at 150 K.

Figure 1 presents the valence-band spectra taken at 170 eV photon energy for the clean $Cu_{84}Al_{16}(100)$ substrate and for different Fe coverages, deposited and measured at 150K. The spectrum of the clean substrate is dominated by the Cu $3d$ band between 5 and 2.5 eV below the Fermi level. In the spectra of the overlayers, the intensity within 1.5 eV from the Fermi level is mostly due to the $3d$ band of iron. The inset shows the intensity decay of the Cu $3d$ band of the substrate as a function of the Fe coverage. The exponential decay indicates that the γ-Fe films cover the substrate uniformly.

Figure 2 shows the Fe $3p$ LMDAD for 4 and 5 ML γ-Fe on $Cu_{84}Al_{16}(100)$, prepared and measured at 150 K with linearly polarized, monochromatic synchrotron radiation of 170 eV. The LMDAD spectra indicate in-plane ferromagnetism at these coverages. Figure 3 shows the evolution of A_{LMDAD} with Fe thickness on $Cu_{84}Al_{16}(100)$. Up to 2 ML, no magnetic order is observed in the direction specified by

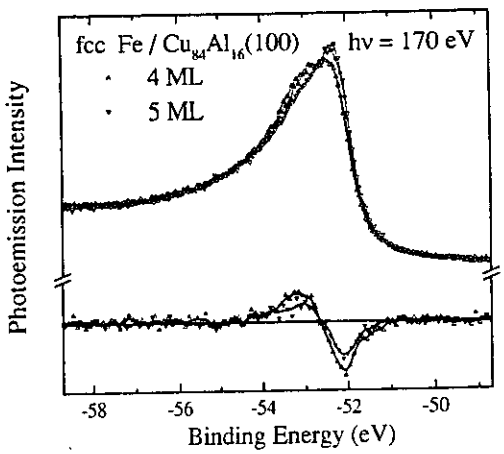

FIG. 2. Fe $3p$ LMDAD spectra for 4 and 5 ML fcc Fe/$Cu_{84}Al_{16}$(100) prepared and measured at 150 K. The existence of magnetic asymmetries indicates in-plane ferromagnetism for the 4 and 5 ML-thick γ-Fe films. Up (down) triangles refer to upward (downward) direction of the sample magnetization with respect to the photoemission plane. Empty (full) symbols refer to the 4 (5 ML) thick iron layer.

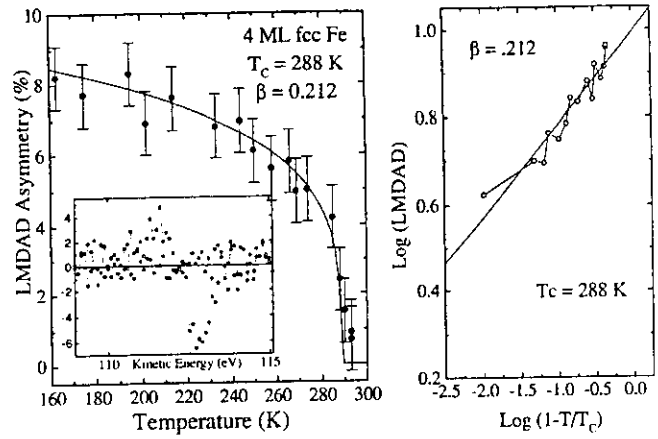

FIG. 4. Temperature dependence of the Fe $3p$ LMDAD for 4 ML fcc Fe on $Cu_{84}Al_{16}$(100). The data are fitted by the power law $[1-(T/T_C)]^{\beta}$. The inset shows the LMDAD asymmetries at 150 K (empty circles) and 300 K (dots). The second panel shows the fitting procedure based on the power-law hypothesis, according to Dürr *et al.* (Ref. 40).

the external applied field (in-plane and perpendicular to the photoemission plane). In-plane ferromagnetism appears at 2.5 ML and A_{LMDAD} reaches a maximum value for 3–4 ML. Assuming that below 2.5 ML our Fe films present perpendicular anisotropy, this result would indicate a lower thickness threshold for the reorientation transition of the ferromagnetic easy axis than reported in the case of a Cu(100) substrate.[20,22,25,37]

The Curie temperature of the in-plane magnetized ultrathin γ-Fe phase has been determined for 4 ML thickness by measuring A_{LMDAD} as a function of temperature, as shown in Fig. 4. The experiment was performed by varying the temperature of the 150 K deposited sample between 150 and 300 K. The data are fitted by a function describing the power-law dependence of the order parameter of ferromagnetism in the neighborhood of the Curie temperature T_C.[38] The fit is obtained by maximizing the function $\log[1-(T/T_C)]$ in the region where log(LMDAD) vs $\log[1-(T/T_C)]$ is linear. This procedure yields an exponent $\beta=0.212(5)$ for the power law $[1-(T/T_C)]^{\beta}$ and a Curie temperature $T_C=288(5)$ K.

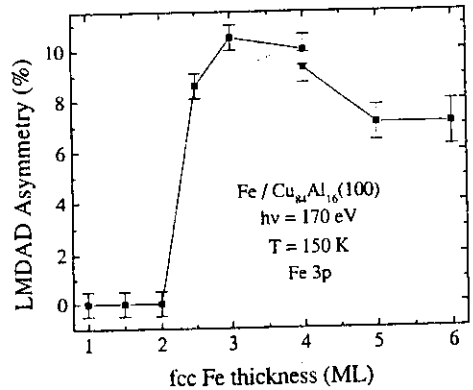

FIG. 3. Fe $3p$ LMDAD asymmetry for increasing Fe coverage on $Cu_{84}Al_{16}$(100), indicating the onset of in-plane magnetization at 2.5 ML Fe and the phase transition between 4 and 5 ML, with 35% reduction of magnetization.

Similar T_C values have been reported for Fe/Cu(100) (Refs. 26 and 15) and Fe/CuAu(111).[11] Our β value agrees well with that predicted by the two-dimensional XY model[39] and with values measured on Fe/Au(100) (Ref. 40) and on Fe/W(100).[41] This extrapolation method for T_C allows for the existence of a deviation from the power law above a certain temperature.[40,42] The deviation is connected to the low dimensionality of the system: in quasi-two-dimensional systems the spin fluctuations related to the phase transition are very important and affect a larger temperature range near T_C than in bulk ferromagnetism. By reaching T_C from below, the magnetization may not vanish because of the formation of short-range ordered spin clusters that can show different T_C values, depending on their size.[43] The spread of the measured A_{LMDAD} values near T_C provides evidence for a limited coherence length that is connected to the high density of defects in the low-temperature grown layer. The possible onset of interdiffusion at the interface, when annealing at room temperature, may have a direct consequence on the deviation from the power-law behavior.

The analysis of the energy splitting of the Fe $3p$ core level can give insight on the *local* magnetic moment of the iron atoms in the epitaxial films. In Fig. 5 we compare the Fe $3p$ LMDAD splitting of 3 ML fcc-Fe on $Cu_{84}Al_{16}$(100) [$\Delta E=1.10(2)$ eV] of a standard bcc-Fe(100) surface. The energy width of the dichroism spectrum represents the energy splitting of the $J=\frac{3}{2}$ multiplet due to the exchange interaction for the $3p$ core hole and the spin-polarized valence band. The splitting reflects therefore the value of the magnetic moment of the excited atom, i.e., a local property.[30,32] Recent experiments on Fe-Co and Fe-Ni surface alloys[34] have demonstrated that the width of the $3p$ core level LMDAD spectra is proportional to the *local* magnetic moment. This means that sizable changes of the iron *local* magnetic moment are reflected in changes of the splitting energy of the core hole magnetic sublevel, and consequently on the width of the LMDAD spectrum. Roughly speaking, the width of the LMDAD spectrum for the predicted low-spin ferromagnetic phase with $1.1\mu_B$ should be reduced to one-

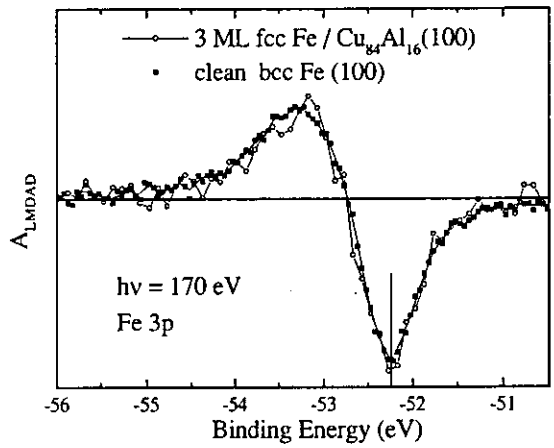

FIG. 5. Fe 3p LMDAD for 4 ML fcc Fe on $Cu_{84}Al_{16}$(100) (open circles) and for bcc-Fe(100) (filled circles). The bcc-Fe(100) spectrum represents the average of a surface enhanced moment of $\sim 3\mu_B$ and subsurface and bulk contributions of $\sim 2.2\mu_B$. According to an escape depth $\lambda = 5(1)$ Å, ~30% of the photoemission intensity originates from the surface and the LMDAD lineshape of bcc-Fe(100) is equivalent to that of a homogeneous Fe film with $\sim 2.5\mu_B$.

half of the width of the LMDAD spectrum for bulk bcc Fe ($2.2\mu_B$). From Fig. 5 we observe that the width of the LMDAD spectrum of 3 ML γ-Fe/$Cu_{84}Al_{16}$(100) and that for the α-Fe(100) are identical within experimental accuracy. A discussion of the LMDAD signal of bcc-Fe is needed at this stage: the reported LMDAD spectra were obtained in highly surface sensitive conditions, which implies that the measured LMDAD line shapes represent the average of surface, subsurface, and substrate contributions.[34] The width of the reference bcc Fe(100) surface spectrum is determined by the surface enhanced moment, the subsurface, and the bulk moments averaged with relative weights set by the surface sensitivity of the measurement. A numerical simulation of the Fe(100) LMDAD spectrum, based on the hypothesis of linear dependence of the LMDAD width upon the magnetic moment and on an escape depth of $\lambda = 5$ Å, gives an average value of the magnetic moment of the sampled bcc iron layers of $2.5(1)\mu_B$. The enhanced values of the magnetic moment at the bcc Fe(100) surface and subsurface layers have been taken from theory ($2.97\mu_B$ for the surface).[44] It appears from Fig. 5 that the magnetic moment of the iron atoms in 3 ML γ-Fe/$Cu_{84}Al_{16}$(100) is of the same value. If we make the hypothesis that the magnetic moment of the 3 ML-thick γ-Fe film is uniform through the layer, then our data are consistent with the formation of the theoretical high-spin ferromagnetic phase characterized by a magnetic moment of $2.5(1)\mu_B$, and with the experimental value from Gradmann and Isbert[11] larger than in bulk α-Fe. In the high-spin state of the γ-phase, iron is a strong ferromagnet, with an almost full majority 3d band. In these conditions, the surface enhancement of the magnetic moment should be limited to a 10% effect at most, likewise in the case of hcp or bcc cobalt.

Above 4 ML, the LMDAD asymmetry is reduced by 35%, as can be seen in Fig. 2. We could not check structural changes on our samples grown on $Cu_{84}Al_{16}$(100), but the reduction of the LMDAD asymmetry signal is consistent with a picture known from (RT grown) Fe/Cu(100): by increasing the Fe thickness, the deeper Fe layers undergo a transformation from a distorted fcc structure towards a more compact undistorted one.[19,22,26,27] If the top layers remain in the perpendicularly expanded, large volume structure, then a magnetovolume instability in the vertical direction may explain the reduction of LMDAD asymmetry (fewer layers in the high spin state) as well as the permanence of a high magnetic moment near the surface. The dense deep layers could be in the antiferromagnetic state at sufficiently low temperature (paramagnetic at 150 K) while the surface/near-surface layers would remain in the high-spin ferromagnetic state with magnetic moments of $2.5(1)\mu_B$. For Fe/$Cu_{84}Al_{16}$(100), the formation of an antiferromagnetically ordered phase in the deep layers for samples thicker than 4 ML is compatible with the LMDAD results, since it would add a nondichroic spectral contribution with a reduced total photoemission peak width (due to the reduced magnetic moment of Fe atoms in the antiferromagnetic phase) to the surface (ferromagnetic) dominated LMDAD spectrum. This contribution cannot severely modify the line shape of the surface sensitive Fe 3p spectra, but can certainly reduce the A_{LMDAD}. On the other hand, if the observed reduction of magnetization for thicknesses larger than 4 ML was due to a transition of the whole γ-Fe film to a low-spin ferromagnetic phase, as suggested by Durrand *et al.* for Fe/Cu(111),[45] then a large reduction of the LMDAD splitting should be observed, which is not the case.

CONCLUSIONS

In conclusion, we have observed in-plane ferromagnetism in ultrathin fcc-Fe(100) layers on $Cu_{84}Al_{16}$(100) for thickness between 2.5 and 6 ML, which were prepared and measured at 150 K. The magnetization is oriented in plane at lower coverage than reported in the studies of Fe/Cu(100), perhaps as a consequence of the laterally expanded $Cu_{84}Al_{16}$(100) lattice, which reduces the need of expanding the interlayer distance perpendicularly in order to reach the favorable atomic volume for the high-spin ferromagnetic phase, and consequently reduces the perpendicular anisotropy. The ferromagnetic fcc-Fe(100)/$Cu_{84}Al_{16}$(100) phase has an average magnetic moment of the order of $2.5\mu_B$, as deduced by comparison with the data from a clean α-Fe(100) surface, and has a Curie temperature close to room temperature for 4 ML thickness. A phase transition is observed between 4 and 5 ML: the order parameter is suddenly reduced but the magnetic splitting of the top layers remains basically unchanged. This can be understood by analogy with the behavior established for γ-Fe/Cu(100) films of similar thickness that exhibit antiferromagnetically ordered (or paramagnetic) deep layers and surface restricted ferromagnetism.

ACKNOWLEDGMENTS

W.A.A.M. and W.N.R. acknowledge the hospitality at LURE during the experiments and the financial support of the Brazilian Agencies CAPES, CNPq, and FAPEMIG. A.S. and W.K. aknowledge financial support by the Deutsche Forschungsgemeinschaft (SFB166). G.R. acknowledges friendly support by H. C. Siegmann.

*Present address: Institut für Metallphysik und Nukleare Festkörperphysik, Technische Universität Braunschweig, 38106 Braunschweig, Germany.

[1] V. L. Moruzzi, P. M. Marcus, and J. Kübler, Phys. Rev. B **39**, 6957 (1989), and references therein.

[2] M. Uhl, L. M. Sandrastskii, and J. Kübler, J. Magn. Magn. Mater. **103**, 314 (1992).

[3] T. Kraft, P. M. Marcus, and M. Scheffler, Phys. Rev. B **49**, 11 511 (1994).

[4] D. Guenzburger and D. E. Ellis, Phys. Rev. B **51**, 12 519 (1995).

[5] J. B. Newkirk, Trans. AIME **209**, 1214 (1957).

[6] W. Keune, T. Ezawa, W. A. A. Macedo, U. Glos, and K. P. Schletz, Physica B **161**, 269 (1989).

[7] W. A. Jesser and J. M. Mathews, Philos. Mag. **15**, 1097 (1967); **17**, 595 (1968).

[8] J. G. Wright, Philos. Mag. **24**, 217 (1971).

[9] U. Gradmann and P. Tillmanns, Phys. Status Solidi A **44**, 539 (1977).

[10] W. Kümmerle and U. Gradmann, Solid State Commun. **24**, 33 (1977); Phys. Status Solidi A **45**, 171 (1978).

[11] U. Gradmann and H. O. Isbert, J. Magn. Magn. Mater. **15-18**, 1109 (1990).

[12] W. A. A. Macedo and W. Keune, Phys. Rev. Lett. **61**, 475 (1988), and references therein.

[13] R. Rochow, C. Carbone, Th. Dodt, F. P. Johnen, and E. Kisker, Phys. Rev. B **41**, 3426 (1990).

[14] W. A. A. Macedo, W. Keune, and R. D. Ellerbrock, J. Magn. Magn. Mater. **93**, 552 (1991).

[15] P. Xhonneux and E. Courtens, Phys. Rev. B **46**, 556 (1992).

[16] F. Baudelet, M.-T. Lin, W. Kuch, K. Meinel, B. Choi, C. M. Schneider, and J. Kirschner, Phys. Rev. B **51**, 12 563 (1995).

[17] W. A. A. Macedo, F. Sirotti, A. Schatz, D. Guarisco, G. Panaccione, and G. Rossi, J. Magn. Magn. Mater. **179–181**, 1262 (1998).

[18] D. J. Keavney, D. F. Storm, J. W. Freeland, I. L. Gricorov, and J. C. Walker, Phys. Rev. Lett. **74**, 4531 (1995).

[19] R. D. Ellerbrock, A. Fuest, A. Schatz, W. Keune, and R. A. Brand, Phys. Rev. Lett. **74**, 3053 (1995); W. Keune, A. Schatz, R. D. Ellerbrock, A. Fuest, K. Wilmers, and R. A. Brand, J. Appl. Phys. **74**, 4265 (1996).

[20] S. Müller, P. Bayer, C. Reischl, K. Heinz, B. Feldmann, H. Zillgen, and M. Wuttig, Phys. Rev. Lett. **74**, 765 (1995).

[21] S. Müller, P. Bayer, A. Kinne, P. Schmailzl, and K. Heinz, Surf. Sci. **322**, 21 (1995).

[22] Dongqi Li, M. Freitag, J. Pearson, Z. Q. Qiu, and S. D. Bader, Phys. Rev. Lett. **72**, 3112 (1994).

[23] M. T. Kief and W. F. Egelhoff, Jr., Phys. Rev. B **47**, 10 785 (1993).

[24] H. Magnan, D. Chandesris, B. Villete, O. Heckmann, and J. Lecante, Phys. Rev. Lett. **67**, 859 (1991).

[25] D. P. Pappas, K. P. Kämper, and H. Hopster, Phys. Rev. Lett. **64**, 3179 (1990).

[26] M. Wuttig, B. Feldmanm, and T. Flores, Surf. Sci. **331-333**, 659 (1995).

[27] J. Thomassen, F. May, B. Feldmann, M. Wuttig, and H. Ibach, Phys. Rev. Lett. **69**, 3831 (1992).

[28] Ch. Wursch, C. H. Back, L. Burgi, U. Ramsperger, A. Vaterlaus, U. Maier, D. Pescia, P. Politi, M. G. Pini, and A. Rettori, Phys. Rev. B **55**, 5643 (1997).

[29] Ch. Roth, F. U. Hillebrecht, H. Rose, and E. Kisker, Phys. Rev. Lett. **70**, 3479 (1993); Solid State Commun. **86**, 647 (1993).

[30] G. Rossi, F. Sirotti, N. Cherepkov, F. Combet Farnoux, and G. Panaccione, Solid State Commun. **90**, 557 (1994); G. Rossi, F. Sirotti and G. Panaccione, in *Core Level Spectroscopies for Magnetic Phenomena: Theory and Experiment, Vol. 345 of NATO Advanced Study Institute*, Vol. 345 *Series B*, edited by P. Bagus, G. Pacchiomi, and F. Parmigiani (Plenum, New York, 1995).

[31] N. A. Cherepkov, Phys. Rev. B **50**, 13 813 (1994).

[32] F. Sirotti, G. Panaccione, and R. Rossi, Phys. Rev. B **52**, 17 063 (1995).

[33] G. Panaccione, F. Sirotti, E. Narducci, and G. Rossi, Phys. Rev. B **55**, 389 (1997); Surf. Sci. **377-379**, 445 (1997).

[34] M. Liberati, thesis Univerità di Modena, Italy 1997; M. Liberati, G. Panaccione, F. Sirotti, P. Prieto, and G. Rossi (unpublished).

[35] F. Sirotti and G. Rossi, Phys. Rev. B **49**, 15 682 (1994).

[36] F. U. Hillebrecht, H. B. Rose, T. Kinoshita, Y. U. Idzerda, G. van der Laan, R. Denecke, and L. Ley, Phys. Rev. Lett. **75**, 2883 (1995).

[37] D. P. Pappas, K.-P. Kämper, and H. Hopster, Phys. Rev. Lett. **64**, 3179 (1990).

[38] A. Aharoni, *Introduction to the Theory of Ferromagnetism* (Clarendon, Oxford, 1996).

[39] S. T. Bramwell and P. C. W. Holdsworth, Phys. Rev. B **49**, 8811 (1994); J. Phys.: Condens. Matter **5**, 53 (1993).

[40] W. Dürr, M. Taborelli, O. Paul, R. Germar, W. Gudat, D. Pescia, and M. Landolt, Phys. Rev. Lett. **62**, 206 (1989).

[41] H. J. Elmers *et al.*, J. Appl. Phys. **79**, 4984 (1996).

[42] D. L. Connely, J. S. Loomis, and D. E. Mapoter, Phys. Rev. B **3**, 924 (1971).

[43] H. C. Siegmann, J. Phys.: Condens. Matter **4**, 8935 (1992).

[44] C. S. Wang and A. J. Freeman, Phys. Rev. B **24**, 4364 (1981); O. Eriksson, G. W. Fernando, R. C. Albers, and A. M. Boring, Solid State Commun. **78**, 801 (1991); S. R. Chubb and W. E. Pickett, Phys. Rev. B **38**, 10 227 (1988).

[45] O. Durrand, J. M. George, J. R. Childress, S. Lequien, A. Schuhl, and A. Fert, J. Magn. Magn. Mater. **121**, 140 (1993).